Resonant sensors for passive, real-time, and wireless characterization of biological analytes

by

Sadaf Charkhabi

A thesis submitted to the graduate faculty

in partial fulfillment of the requirements for the degree of

MASTER OF SCIENCE

Major: Chemical Engineering

Program of Study Committee:
Nigel Reuel, Major Professor
Marshall McDaniel
Qun Wang

The student author, whose presentation of the scholarship herein was approved by the program of study committee, is solely responsible for the content of this thesis. The Graduate College will ensure this thesis is globally accessible and will not permit alterations after a degree is conferred.

Iowa State University

Ames, Iowa

2018

DEDICATION

This thesis is dedicated to my parents and my fiancé who have been a great source of inspiration and support.

TABLE OF CONTENTS

Page

LIST OF FIGURES v

LIST OF TABLES viii

NOMENCLATURE ix

ACKNOWLEDGMENTS x

ABSTRACT xi

CHAPTER 1. INTRODUCTION 1
1.1 Background and Research Objectives 1
1.2 Thesis Structure 3

CHAPTER 2. LITERATURE REVIEW 5
2.1 Biosensors 5
2.1.1 Definition 5
2.1.2 Categories of Biosensor 5
2.1.3 Wireless Biosensor 6
2.1.4 Radio Frequency Identification Systems 7
2.1.4.1 Types of RFID systems 7
2.1.4.2 RFID in sensors 8
2.1.5 Resonant Sensors 8
2.1.5.1 Scattering parameters 9
2.1.5.2 Resonant frequency 10
2.2 Measurement of Hydrolytic Enzyme Activity 10
2.2.1 Hydrolytic Enzymes 10
2.2.1.1 Hydrolytic enzyme market 11
2.2.1.2 Industrial application of hydrolytic enzymes 11
2.2.1.3 Natural processes including hydrolytic enzymes 11
2.2.2 Assays for Enzyme Activity Measurement 12

CHAPTER 3. METHODOLOGY 13
3.1 Materials 13
3.2 Sensor Setup Design 13
3.2.1 Resonator Fabrication 13
3.2.2 Reader Design 17
3.3 Sensor Response Monitoring Procedure 18
3.3.1 Resonator Detection 18
3.3.2 Substrate Coated Resonator Fabrication 19
3.3.3 Bead Test for the Resonant Frequency and Radius Correlation 20
3.3.4 Testing Substrate Coated Resonators 21
3.3.5 Soil Tests 21

CHAPTER 4. RESULTS AND DISCUSSION 23
4.1 influence of resonator geometry on the start resonant frequency 23
4.1.1 Length Effect 23
4.1.2 Pitch Effect 25
4.2 Effect of Relative Permittivity on Resonant Frequency 27
4.3 Design of Hydrolytic Enzyme Activity Measurement Tests 28
4.3.1 Purified Subtilisin A Test 31
4.3.2 Unpurified Bacterial Protease Test 32
4.4 Modeling 33
4.4.1 Bead Test for Modeling 36
4.4.2 Transport Model for Subtilisin A 40
4.4.3 Transport Model for Bacterial Protease 43
4.5 Effect of Hydrogel Composition on Sensor Response 45
4.6 Soil Test 48

CHAPTER 5. CONCLUSION AND FUTURE WORK 52

REFERENCES 58

APPENDIX. MATLAB SCRIPTS 65
1. Matlab Code for VNA Signal Capture 65
2. Matlab Code for Resonant Frequency Detection 70
3. Code for the Numerical Model 71
4. Code for Bead Experiment Image Analysis 73

LIST OF FIGURES

Page

Figure 1 The Archimedean coil designed with a specific pitch, length, and diameter on computer CAD software. 14

Figure 2 The trace is drawn as a positive mask on the copper substrate using an XY plotter and indelible marker..... 15

Figure 3 Use of acetone for releasing the resonant sensor after the etching process..... 15

Figure 4 Schematic diagram of resonant sensor epoxied to the petri dish..... 16

Figure *5* Two loop reader with different loop diameters for optimizing the reader geometry. 17

Figure 6 Two loop reader antenna designed with CAD software and 3D-printed. 18

Figure 7 Rapid prototyping of flexible resonant sensors using Pyralux and reading the scattering parameter using reader antenna connected to the VNA..... 19

Figure 8 Preparation of gelatin substrate. 20

Figure 9 Substrate Coated resonator using an O-ring. 20

Figure 10 Pink fluorescent beads used for the empirical relation of resonant frequency to radius measurements. 21

Figure 11 Constant pitch (1.2mm) resonant sensors with various lengths (407-2764mm)..... 23

Figure 12 Effect of resonator length on the sensor response and the resonant frequency of the sensor..... 24

Figure 13 Power model fit on the experimental resonant frequency responses for different length sizes of the sensors..... 24

Figure 14 Fabricated resonant sensors with constant length (1255mm) and a pitch size range of 1-2.5mm. 25

Figure 15 Effect of resonant sensor pitch size on the S_{21} magnitude response and the resonant frequency of the sensor. 26

Figure 16 Resonant sensor response (S_{21} magnitude) for materials with different relative permittivity. 27

Figure 17 Comparison of the resonant frequency changes of the standard resonator having deionized water vs vegetable oil on the resonator's surface..... 28

Figure 18 Design of the substrate-coated resonant sensor for hydrolytic enzyme activity and the digestion of the substrate. 29

Figure 19 S_{21} magnitude response curves for gelatin, gelatin with enzyme, and gelatin after digestion. 30

Figure 20 Resonant sensor response for different concentrations of Subtilisin A..... 31

Figure 21 Effect of bacterial protease concentration on the resonant frequency response of the sensor..... 32

Figure 22 Simplified mass balance problem by reducing the problem to radial coordinates..... 34

Figure 23 Change in resonant frequency during digestion with tracker beads in the center well (inserts show screenshots from video of the control sample and digested sample). 37

Figure 24 Reactive front radius vs. time data extracted from digested bead video with accompanying quadratic fit. 38

Figure 25 Relation of frequency drop to the reactive front radius..... 39

Figure 26 Digest model simulations at various enzyme concentrations for 1000s..... 39

Figure 27 Developed digest model for different enzyme turnover rates. 40

Figure 28 The changes in enzyme well radius corresponding to experimental data for purified Subtilisin A..... 41

Figure 29 The model fit on the first 1000(s) of the experimental data for Subtilisin A. 42

Figure 30 The changes in enzyme well radius corresponding to experimental data for the unpurified bacterial protease..... 44

Figure 31 Transport model fit for different concentrations of unpurified bacterial protease..... 45

Figure 32 Effect of gelatin wt% on sensor response trajectory, gelatin structure is shown as insert. 46

Figure 33 Model fit for different gelatin concentrations. 47

Figure 34 Plasticizer wt% effect on sensor response. 48

Figure 35 The sensor response for autoclaved soil, regular soil, and soil with the added enzyme. 49

Figure 36 Digest model fit for soil at k_{cat} = 0.00152 s^{-1}(soil basis) and D = $1.2 \cdot 10^{-6}$ cm^2/s. 50

Figure 37 Plastic casing used to isolate resonator in soil tests. 51

Figure 38 S_{21} magnitude (dB) response to KCl added to 40mm diameter, 1mm pitch resonators. 55

Figure 39 Effect of resonator geometry on the sensor S_{21} response to KCl concentrations for resonators with constant length and different pitch sizes. 55

Figure 40 Effect of resonator geometry on the sensor S_{21} response to KCl concentrations for resonators with constant pitch and different length sizes. 56

Figure 41 S_{21} magnitude and phase presented in polar plots for four different ionic compounds. 57

LIST OF TABLES

Page

Tabel 1 Dimensions of the resonators designed using CAD software..... 14

Table 2 Resonator specifications. 16

Table 3 K_{cat} values for different concentrations of Subtilisin A. 42

Table 4 K_{cat} values for different concentrations of unpurified bacterial protease. 44

Table 5 Resonator geometry panel used for KCl and different ionic compounds(*). 54

Table 6 Salt panel for testing ion selectivity response of the resonant sensors. 56

NOMENCLATURE

AIS	Automatic Identification System
BNC	Bayonet Neill Concelman
DOF	Degree Of Freedom
FET	Field Effect Transistor
GOx	Glucose Oxidase
PBS	Phosphate Buffered Saline
POC	Point Of Care
RFID	Radio Frequency Identification
SAW	Surface Acoustic Wave
SPR	Surface Plasmon Resonance
TELISA	Thermometric-biosensor to Enzyme-Linked Immunosorbent Assay
VIN	Vehicle Identification Number
VNA	Vector Network Analyzer

ACKNOWLEDGMENTS

A depth of gratitude is owed first and foremost to Prof. Nigel Reuel for providing me with the opportunity to work under his supervision. This thesis would not have been possible without his persistent support, generous guidance, encouragement, and friendship.

I would like to thank my committee members, Prof. Qun Wang, and Prof. Marshall McDaniel for their invaluable help throughout the course of this research.

In addition, I would like to thank my beloved family for their endless support throughout my life. Although they are thousands of miles away, their immeasurable love is the main inspiration I take with me every day. And I would like to thank my fiancé, Peyman, for his unconditional support, patience, care, and understanding.

ABSTRACT

A passive, low-cost resonant sensor was developed with the potential application of wireless monitoring of hydrolytic enzyme activity in closed systems. The resonators are rapidly prototyped from polyimide substrates (25μm thickness) which are coated with a thin layer of copper (35μm thickness). The patterns of the resonators, which are Archimedean spirals, are drawn on these substrates using an indelible marker with an XY plotter. These substrates are etched with a solution containing hydrogen peroxide and hydrochloric acid in order to remove the undesired copper.

The initial resonant frequency of these resonators can be controlled by the Archimedean coil length and pitch size of the spiral. The frequency response window is tuned for the 1-100 MHz range for better penetration through soil, water, and tissue. The resonant frequency can be measured up to 5cm stand-off distance by a 3D-printed coplanar, two-loop coil reader antenna. This reader is attached to a vector network analyzer for monitoring the magnitude of S_{21} scattering parameter. The central hypothesis is that the Archimedean spiral sensors respond to any change in relative permittivity of the medium in contact with the resonator. This response is represented as a clear shift in the resonant frequency of the resonator. For instance, changing the medium from air to water results in approximately 50MHz redshift in the resonant frequency.

In order to measure hydrolytic enzyme activity, the resonant sensors are coated by an enzyme substrate (e.g. hydrogel). The degradation of the enzyme substrate causes a change in the relative permittivity which results in a shift in the resonant frequency (up to 7MHz redshift). By fitting a transport-reaction model, which simulates the radial

digestion profile, on the experimental data the activity (turnover rate, or k_{cat} value) of the enzyme is calculated. This approach is used for testing purified Subtilisin A and unpurified bacterial protease samples at different concentrations ranging from 30mg/ml to 200mg/ml with k_{cat} values of 0.003-0.002 and 0.009-0.004 $g_{substrate}/g_{enzyme}$ per second, respectively. The sensor response rate can be tuned by changing the substrate composition (i.e. changing the gelatin and glycerol plasticizer weight percentage in the hydrogel). Finally, the applicability of these resonant sensors in a real-life problem is demonstrated by wirelessly measuring the proteolytic activity of farm soil with a measured k_{cat} of 0.00152 $g_{substrate}/(g_{soil} \cdot s)$ using 3D-printed plastic cases.

CHAPTER 1. INTRODUCTION

1.1 Background and Research Objectives

Biosensors, which are devices used for detecting biological components, have played an important role in various industries in the past few decades. These sensors can have immense applications in food safety, agriculture, water quality, disease screening and healthcare monitoring, environmental pollution control, and pathogen detection. The history of biosensors goes back to the invention of oxygen probe by L. C. Clark for oxygen detection followed by blood glucose measurement via an amperometric enzyme electrode.[1] This biosensor was the first generation of glucose oxidase (GOx) biosensors which are still known as the most widely used biosensors all over the world.[2]

In recent years, there has been a push for developing new techniques to help with overcoming the limitations of traditional biosensors. The most important constraint of commercially-available biosensors is that they are not cost-effective, and most of them do not exist in a wireless form. These issues are known as critical problems in places in which multiple sensors are required in order to capture enough data for accurate analysis, such as a corn field. Moreover, having a contact-required biosensor is difficult or impractical in some applications such as a bioreactor.

There are many examples of wired sensors that can be rendered wireless by coupling to communication circuitry (e.g. Wi-Fi, Bluetooth, infrared, and cellular).[3] Examples include sensors used for weather monitoring, transportation, healthcare, animal tracking, and food inspection.[4] A wireless sensor for hydrolytic enzyme activity could use a similar approach, such as coating the surface of a field effect transistor (FET) with the substrate of the target

enzyme; however, the cost of the included circuitry would raise the per unit price significantly and limit adoption and use in applications that require high-frequency measurements. For an ultralow-cost (e.g. disposable) sensor, a new sensor platform must be used such as the resonant sensors described here.

The purpose of this work was to design a low-cost, resonant sensor to measure hydrolytic enzyme activity in a closed system. In doing so, a novel rapid prototyping method for flexible resonant sensors was developed using an XY plotter, indelible marker, and copper coated flexible substrates. A two loop antenna, coplanar reader was designed and 3D-printed to enable wireless communication with the resonators. An optimized enzyme substrate material composition and fabrication method were then determined to transduce enzyme activity. A model was designed to relate the rate of the substrate degradation to enzyme activity. Finally, a proof of concept device was constructed to demonstrate the utility of these new resonant sensors in measuring hydrolytic enzyme activity of soils.

This new sensor is relevant, arguably critical, to soil enzymology because the current methods used for soil enzymatic activity (namely fluorometric and colorimetric assays[5,6]) are tedious methods which are not capable of capturing *in situ* activity measurements (i.e. soil samples must be collected in the field and analyzed in the lab). These methods create an artifact of measuring potential enzyme activity and not the real activity. Therefore, an inexpensive, contact-free sensor would give us the ability not only to measure soil enzyme activity repeatedly in multiple locations in a field, but also with high frequency through time. Increasing the sampling density in space and frequency in time will help better quantify and understand the large spatiotemporal variability of carbon and nutrient cycling in soils, and

thus improve management of soils in order to reduce environmental pollution (whether greenhouse gas emissions or nutrient leaching).

The overall objectives of this study can be summarized as follow:

1. Design and develop a new class of resonant sensors.
2. Optimize the sensor and reader antenna geometry.
3. Evaluate the sensor response for enzyme activity measurement.
4. Validate the applicability of the sensor using soil as a test case.

1.2 Thesis Structure

This thesis is organized into five main chapters. A brief description of these chapters are as follow:

Chapter 1: Introduction — in this chapter a concise background of the biosensor is provided. Additionally, the limitations of the traditional biosensors are described and the need for further research on the wireless sensors is outlined. The main objectives of this research are briefly explained.

Chapter 2: Literature Review — in the first part of this chapter, the biosensor is defined and its categories are explained. Also, the wireless biosensors and the application of radio frequency identification systems in developing resonant sensors as well as the key parameters of resonant sensors (scattering parameters and resonant frequency) are well-defined. In the second half of the chapter, hydrolytic enzymes and their significant role both in nature and a variety of industries are explained. The established methods for

measuring the hydrolytic enzyme activity, such as fluorometric assay, are described as well.

Chapter 3: Methodology — first, the materials used for the experiments conducted in this research are described. The fabrication of resonators and the reader setup are demonstrated and the procedures for applying the resonant sensor for measuring the hydrolytic enzyme activity of Subtilisin A, bacterial protease, and use within a typical loam soil from central Iowa are explained.

Chapter 4: Results and Discussion — this chapter is structured into 6 main sessions. First, the effect of the resonator geometry (i.e. coil length and pitch size) and the relative permittivity of the dielectric medium close to the sensor on the resonant frequency is studied. Next, the sensor response regarding the substrate degradation for different concentrations of purified Subtilisin A and unpurified bacterial protease are provided. Moreover, the effect of substrate composition on the dynamic response time of the sensor is explored. Then, the transport model is fitted on all of the empirical data for measurement of enzyme k_{cat} value. Finally, the sensor and the model are used for measuring the soil hydrolytic activity.

Chapter 5: Conclusion — the conclusion of this study is presented in the final chapter. Moreover, the potential future direction of this research is proposed.

CHAPTER 2. LITERATURE REVIEW

2.1 Biosensors

2.1.1 Definition

A biosensor is a device which is selectively sensitive to either concentration or activity of a chemical in a biological sample.[7] In other words, biosensors provide us with information regarding biophysical or biochemical properties of a system.[8] Similar to other chemical sensors, biosensors consist of a receptor and a transducer which make the system capable of producing a measurable signal proportional to the concentration of desired analyte present in the sample.[9] Therefore, the biosensor can also be defined as a sensor in which the receptor part is based on biochemical principles.[10]

2.1.2 Categories of Biosensor

Among many ways to categorize biosensors, classifying them based on their transduction method is the most common one. Optical, electrochemical, mass-sensitive, and thermal sensors are the most typical types. [9] Each category is briefly explained below:

1. Optical biosensors: the optical biosensors, known as the most common type of biosensors, are self-sufficient comprehensive sensors working based on reflection, absorbance, surface plasmon resonances (SPR), photoluminescence, etc.[11,12] One of the interesting explored applications of the optical sensor was detecting *E. coli* using fluorescent pH-responsive polymeric micelles which were bioconjugated to anti *E. coli* as the capturing agent.[13]

2. Electrochemical biosensors: in these types of biosensors, an interaction between electricity and chemistry leads to a response.[14] Among traditional techniques used

in electrochemical sensing, cyclic voltammetry, chronopotentiometry, and impedance spectroscopy are the most common methods.[2] one of the most recent techniques mostly rely on nanotechnology such as nanowire-based electrochemical biosensors.[15]

3. Mass-sensitive biosensors: the measurement of variations of the mass or any other property that can be scaled proportionally to mass is used for analyte sensing in this type of biosensors.[14,16] For instance, molecular binding events can be detected using a mass-sensitive surface acoustic wave (SAW) biosensor working based on the piezoelectric property of the sensor.[17]

4. Thermal biosensors: these sensors operate based on the measurement of absorbed or released thermal energy in a biochemical reaction without the need for labeling the reactants.[18] Thermal sensors can be used for a variety of applications including determination of biomolecules such as hormones using thermometric biosensor to enzyme-linked immunosorbent assay (TELISA).[19]

2.1.3 Wireless Biosensor

The invention of wireless biosensors has been a breakthrough in sensor fields by enabling researchers with continuous monitoring of analytes in places which are tedious or even impossible to have a contact-required communication for the biosensor. One of the first applications of wireless biosensors was for in vivo pH measurement in 1990's.[20] In addition, researchers were able to monitor blood glucose of flatfish under its normal free swimming condition by implanting a needle wireless biosensor in a flatfish's interstitial fluid.[21] The most important application of wireless biosensors is the point of care (POC) in the medical

field for cancer detection, genetic disorder diagnosis, and blood-glucose monitoring which is known as the most commercially prevalent biosensor.[22]

2.1.4 Radio Frequency Identification Systems

One of the technologies which have influenced the wireless biosensor field over the past few decades is radio frequency identification (RFID) which is a type of automatic identification system (AIS). AISs are a broad class of devices used as a substitute for time-consuming manual data verification methods and play an essential role in modern world. Barcodes on products, vehicle identification numbers (VIN) in cars, credit cards, access cards, and biometric systems are some of the common AISs we use in our everyday lives. RFID technology is a rapidly growing method for wireless and contact-free data collection using electromagnetic waves for data communication.[23]

2.1.4.1 Types of RFID systems

RFID systems can either be categorized as active RFIDs by having an internal power source such as a battery, or passive RFIDs which do not have any electrical source installed within the system and are powered based on the radio frequency they receive from the reader.[24–26] The most important advantages of passive RFIDs over active RFIDs is that the passive one is a cheaper smaller maintenance-free device with a longer operational life; however, the limitations of passive RFID systems, such as communicating over lower distances and having fewer identification capabilities in comparison with the active system, should not be neglected.[24]

2.1.4.2 RFID in sensors

RFID tags helped with the invention of passive resonator wireless sensors, consisting of an inductor-capacitor (LC) circuit as well as an external reader antenna, used for several applications.[27] Deposited single-walled carbon nanotube film in a chipless RFID antenna was used for wireless detection of toxic gases such as ammonia and nitrogen oxide.[28] Coupling an integrated humidity sensor with an LC circuit and pairing it with an external reader antenna led to the invention of a sensitive single-chip passive wireless humidity sensor.[29] The development of multiple passive microsensors helped the wireless detection and measurement of hazardous materials in the water systems.[30] Analyte-activated swelling of hydrogel was used for changing the capacitance of the LC circuit and wirelessly measuring the concentration of calcium nitrate tetrahydrate.[31] Using a photosensitive polymer, researchers were able to make an RFID tag for wireless detection of light exposure in goods which are sensitive to light.[25] All of these systems operate based on a signal sent from RFID reader to the tag, a backscattered signal sent from the tag to the reader, the process of the backscattered signal, and recognition of spectral properties of the tag.[32]

2.1.5 Resonant Sensors

Resonant sensors are simple, low-cost circuits composed of an inductor (L), capacitor (C) and inherent system resistance (R) that tunes the circuit to a specific resonant frequency; by altering one or more of the circuit parameters upon analyte binding or analyte activity, the resonant frequency changes. The sensor transduction is observed by interrogating the sensor with a vector network analyzer to monitor changes in the resonant frequency (or more specifically, the transmission scattering parameters S_{11}, S_{22}, S_{21}, and S_{12}). These resonant sensors (also called LC or LCR sensors) have been demonstrated for several applications.[27]

For instance, Ong et al. designed a wireless passive LC resonator and applied it for monitoring pressure, temperature, and humidity of the sensor's environment.[33] More recent work demonstrated the ability to transduce a signal regulated by enzyme allostery using a screen-printable resonant sensor.[34]

2.1.5.1 Scattering parameters

There are several circuit matrix representations used for characterizing the circuits at different frequency regions.[35] The prominent examples of these matrices are admittance parameters (Y-parameters), impedance parameters (Z-parameters), hybrid parameters (H-parameters), and scattering parameters (S-parameters).[36] S-parameters are mostly used in microwave and radio frequency ranges. For an N-port network, the S-matrix would be represented as an N by N square consisting N^2 elements. For a two-port vector network analyzer, for example, the S-matrix is:

$$S = \begin{bmatrix} s_{11} & s_{12} \\ s_{21} & s_{22} \end{bmatrix} \quad (1)$$

Where S_{11} and S_{22} are defined as the reflection coefficients (the ratio of the reflected wave to the incident wave) for port 1 and 2, respectively. S_{12} represents the power which is transferred from port 2 to port 1 and S_{21} is the ratio of the amplitude of the transmitted wave through port 2 to the amplitude of the incident wave from port 1. Each of these S-parameters is a complex number representing amplitude and phase. The unit of the amplitude of the S-parameter is decibels (dB) which can be easily converted to power or voltage using the following equations:[37]

$$\mathrm{dB} = 10\log\frac{\text{power}}{\text{reference power}} \tag{2}$$

$$\mathrm{dB} = 20\log\frac{\text{voltage}}{\text{reference voltage}} \tag{3}$$

For instance, S_{21}=0dB means that all the power delivered to port 1 is 100% transmitted to port 2.

2.1.5.2 Resonant frequency

The resonant frequency is defined as the specific frequency in which the resonator naturally oscillates. The number of resonant frequencies that a physical system can potentially have is based on the degree of freedom (DOF) of the system.[38] A tuned LC circuit, for instance, has one degree of freedom and hence can only have a single resonant frequency.[39] All resonators have the ability to resonate at multiple frequencies, which are harmonic frequencies of the original resonant frequency. The relationship between these frequencies is dependent on the resonator's design. For a disk planar Archimedean spiral resonator, the first fundamental harmonic frequency is denoted as f_1 and the higher resonant frequency modes can be roughly calculated by the following equation:[40]

$$f_n \sim \mathrm{n}f_1 \tag{4}$$

In which n= 1, 2… and represents the resonance mode.

2.2 Measurement of Hydrolytic Enzyme Activity

2.2.1 Hydrolytic Enzymes

Enzymes are defined as protein catalysts known for both their specificity and ability to increase the rate of chemical reactions via providing the reaction with an alternative

pathway with lower activation energy. In addition, enzymes are neither consumed nor undergo any dramatic alterations during the reaction.[41–43] Hydrolytic enzymes are type of enzymes which catalyze the hydrolysis of a chemical bond.

2.2.1.1 Hydrolytic enzyme market

Hydrolytic enzymes are critical biocatalysts used in natural and industrial processes. Approximately 75% of enzymes used in industry are hydrolases with proteases, lipases, and carbohydrases as the most commercially used types in the enzyme market.[44] Industrial enzymes had an estimated global market of US $4.2 billion in 2014 and it is anticipated that their market size will reach US $6.2 billion having almost 7% compound annual growth rate.[45,46]

2.2.1.2 Industrial application of hydrolytic enzymes

Industrial processes with hydrolytic enzymes include leather tanning, paper industry, starch and fuel, juice clarification, cheesemaking, brewing, wastewater treatment, cosmetic industry, and detergent manufacturing.[44,47–50] It is noteworthy to mention that almost 60% of the enzyme market is related to commercial proteases.[51]

2.2.1.3 Natural processes including hydrolytic enzymes

Examples in nature include soil enzymes such as protease, urease, cellulase, and phosphatase that render organic compounds into mineralized forms of nitrogen, sulfur, and phosphorus for plant growth.[52,53] They are key indicators of soil health[54,55] and can be used to as an integrated measure of soil microbial activity or as an indicator of supply and demand of carbon and nutrients.[56–58] Notwithstanding the importance of hydrolytic enzymes, *in situ* measurement of their activity still remains a challenge due to laborious methods and

difficulty in translating potential soil enzyme activity measured in a laboratory with *in situ* activity.[59–61]

2.2.2 Assays for Enzyme Activity Measurement

Many assays have been developed to characterize enzyme activity *ex-situ* in lab-based techniques.[62] Enzyme catalytic activity (k_{cat} or turnover frequency) is defined as the mass of substrate consumed per mass of enzyme for a given time period. Among several established methods for determining the enzyme activity, fluorometric and colorimetric are the most common assays used.[5,6] For example, a synthetic substrate which is usually C-, P-, or N-rich bonded to a fluorescent dye is used to measure the soil extracellular enzyme activities.[63] An example of colorimetric enzyme assay is measurement of calpain (a proteolytic enzyme) activity in the visible range (595nm) by using Coomassie brilliant blue G-250 dye reagent.[64] Although colorimetric assays are easier to perform since the signal is a visible change in the reaction's color, fluorometric methods are more frequently used due to their higher sensitivity.[65]

A major limitation for each of these existing assays is the requirement of sample collection; this becomes a problem for closed systems where such sampling is inconvenient or impossible. Examples of closed systems with enzyme activity are bioreactors, soil environments, and bandages;[52,66,67] each would benefit from wireless sensors capable of probing closed systems.

CHAPTER 3. METHODOLOGY

3.1 Materials

Bacterial protease, gelatin, and hydrogen peroxide (H_2O_2, 3%) were purchased from Carolina Biological Supply Company. Hydrochloric acid (HCl) and acetone (C_3H_6O) were procured from Fisher Scientific. Protease from *Bacillus licheniformis* (Subtilisin A, 7-15 units/mg solid) and red fluorescent amine-modified polystyrene latex beads (aqueous suspension, 1.0µm mean particle size) were bought from Sigma-Aldrich and glycerol ($C_3H_8O_3$) was purchased from VWR. Dupont Pyralux AC flexible sheet and a Silhouette Curio XY plotter were utilized for resonator fabrication. An S5048 two-port vector network analyzer from Copper Mountain Technologies was used to measure the resonant sensor scattering parameters. This was coupled to a two loop antenna constructed in a custom, 3D-printed housing using an Airwolf Axiom 3D printer. The 3D printer was also used to print resonant sensor cases for soil testing. A Logitech C920 HD Pro Webcam was used for time-lapse photography.

3.2 Sensor Setup Design

3.2.1 Resonator Fabrication

The initial focus of this research was designing the resonator's structure. Spirals with different pitches in the range of 1-2.5mm and coil lengths of 407-2764mm, which resulted in resonators of outer diameters 15-60mm sizes, were designed using Rhino 5 software (Fig 1). The dimensions of the designed spirals are shown in Table 1.

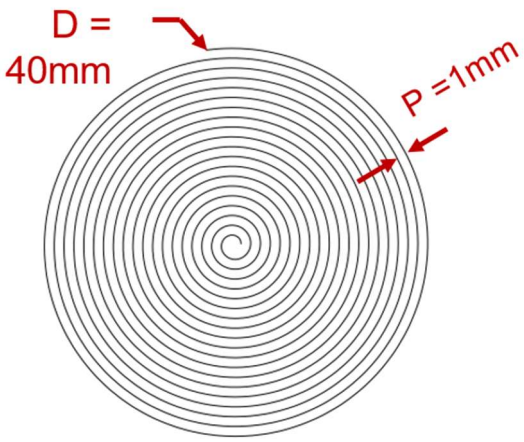

Figure 1 The Archimedean coil designed with a specific pitch, length, and diameter on computer CAD software.

Using the Silhouette Curio printer with a Sharpie ultra fine point permanent marker, spirals were drawn on Dupont Pyralux printed circuit board flexible polyimide (25µm) with a thin layer of copper (35µm) (Fig 2).

Tabel 1 Dimensions of the resonators designed using CAD software.

Specification	Pitch (mm)	Length(mm)	Outer Diameter (mm)	Inner Diameter (mm)
Constant Length	1	1255.129	40	1.5
	1.2	1255.038	43.81	1.5
	1.6	1255.659	50.59	1.5
	2	1255.06	56.54	1.5
	2.5	1255.255	63.21	1.5
Constant Pitch	1.2	407.856	25	1.5
	1.2	800.587	35	1.5
	1.2	1324.211	45	1.5
	1.2	1978.728	55	1.5
	1.2	2764.142	65	1.5

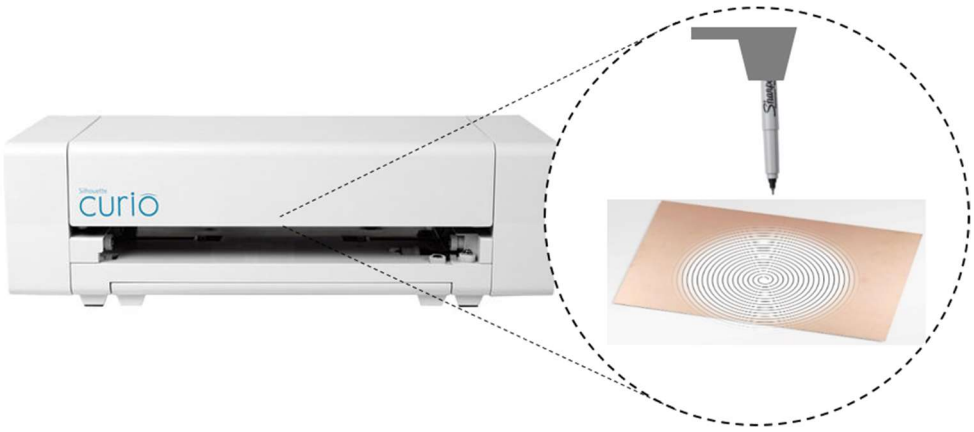

Figure 2 The trace is drawn as a positive mask on the copper substrate using an XY plotter and indelible marker.

The Pyralux sheet was subsequently etched using a solution of hydrogen peroxide and hydrochloric acid with a 2:1 ratio (i.e. 15ml of HCl was added to 30ml of H_2O_2 for each resonator) in the fume hood. The optimal etching time to prevent over-etching of the masked spiral trace while removing the undesired copper was found to be 15 to 25min depending on the size of the resonator. The etched Pyralux was then rinsed with acetone to remove the permanent marker (Fig 3).

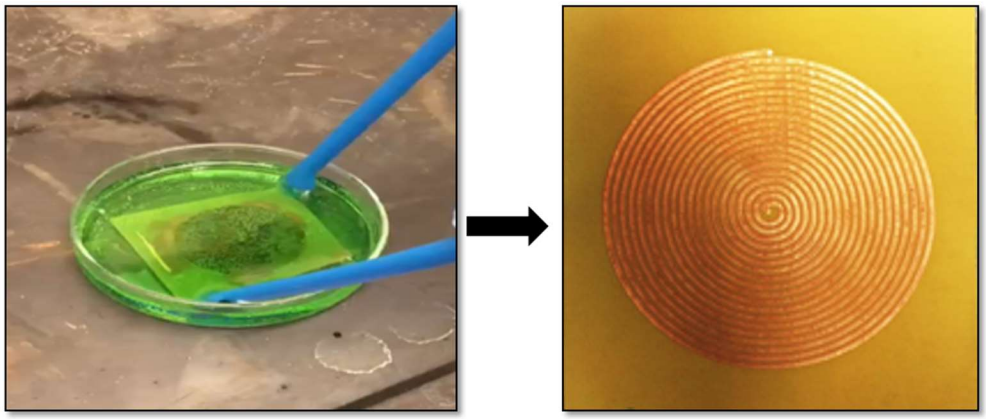

Figure 3 Use of acetone for releasing the resonant sensor after the etching process.

The flexible resonator was then inverted and epoxied on a petri dish to protect the resonator from electrically shorting; in this mode, the polyimide film becomes the sensor surface (Fig 4).

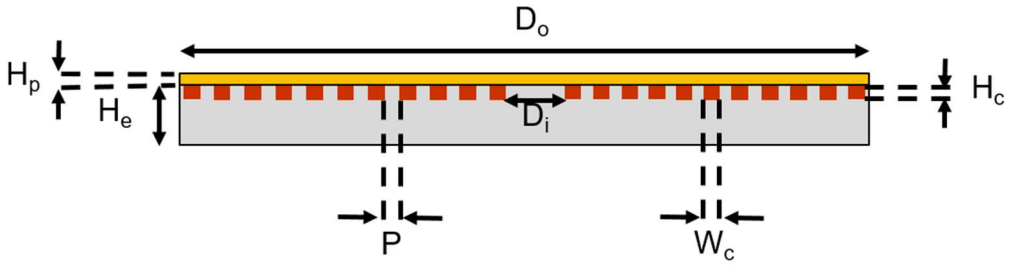

Figure 4 Schematic diagram of resonant sensor epoxied to the petri dish.

Each of the symbols shown in the schematic diagram is explained and the dimension ranges are shown in Table 2.

Table 2 Resonator specifications.

Symbol	Definition	Dimension
D_o	Outer spiral diameter	15 to 60mm
D_i	Inner spiral diameter	1.5mm
P	Spiral pitch	1 to 3mm
W_c	Copper width	~1mm
H_c	Copper height	35µm
H_p	Polyimide height	25µm
H_e	Epoxy height	~ 1mm

This process allowed for rapid prototype development in our own lab with the trade-off being larger feature sizes (down to 200µm can be resolved). Smaller features can be made via screen printing or lithographic mask techniques, albeit at a longer lead time between new designs.[68–71]

3.2.2 Reader Design

A two loop antenna, coplanar reader was designed and 3D-printed enabling wireless communication with the resonators. The loop size was optimized based on the signal clarity of the sensor response with minimum background noise after trying several diameters (Fig 5). Moreover, the reading range of the reader for different loop sizes was taken into consideration when optimizing the reader geometry. In the final design, each of the copper wire loops had a diameter (D) of 54mm, and the two loops had an overlap (E) of 26.7mm along the center axes (Fig 6). The copper wires were soldered to the Bayonet Neill Concelman (BNC) plugs and mutually grounded to minimize the effects of cable length and position.

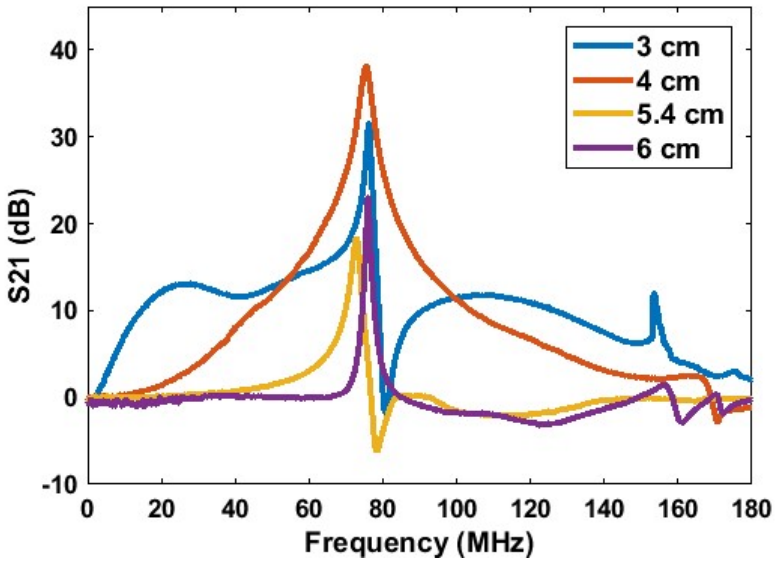

Figure *5* Two loop reader with different loop diameters for optimizing the reader geometry.

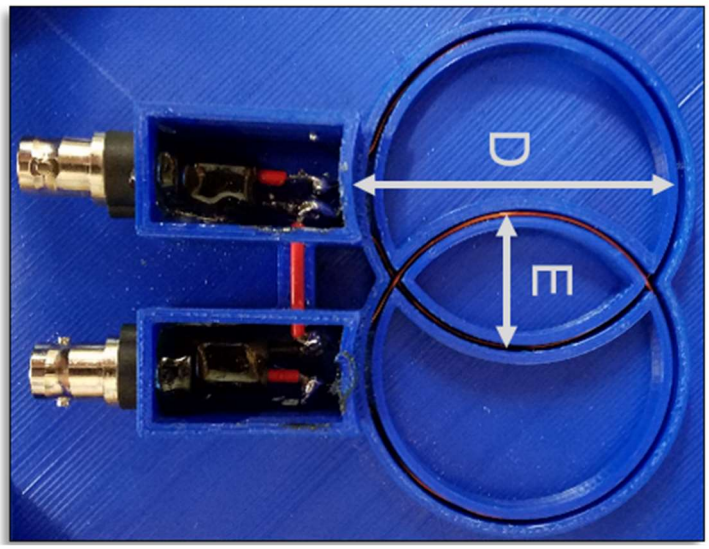

Figure 6 Two loop reader antenna designed with CAD software and 3D-printed.

3.3 Sensor Response Monitoring Procedure

3.3.1 Resonator Detection

As it was mentioned, the resonant frequency of the resonator was measured using two copper loop antennas set in a 3D-printed reader frame; this was connected to a two-port vector network analyzer (VNA). For studying the response of this class of resonant-based sensors, the magnitude of S_{21} in a frequency range of 1-100MHz was monitored. The standard resonator geometry used in the measurements was the spiral with an outer diameter of 40mm, an inner diameter of 1.5mm, and a pitch of 1mm having a resonant frequency of approximately 75MHz in the air. The BNC plugs used in the reader antenna were connected to the VNA ports using RF-shielded and immobilized sets of BNC cables. The mutual inductance coupling between the resonant sensor and the reader coils was sufficiently strong to provide a clear S_{21} signal up to a 5cm stand off distance in the air. The VNA was connected to a Lenovo laptop with Windows OS and the VNA data acquisition was automated via Matlab (Appendix A.1 for scripts).

The resonant frequency was identified as the peak of the characteristic S_{21} magnitude sigmoidal response (Appendix A.2 for scripts). In general, the process of resonator fabrication and resonant frequency detection technique is summarized in Figure 7.

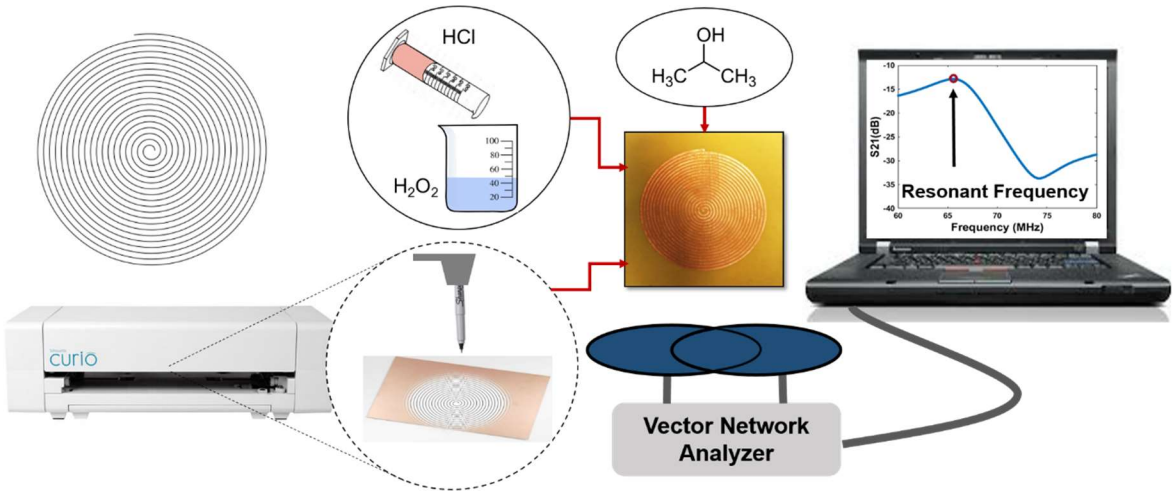

Figure 7 Rapid prototyping of flexible resonant sensors using Pyralux and reading the scattering parameter using reader antenna connected to the VNA.

3.3.2 Substrate Coated Resonator Fabrication

3.5 to 15g Gelatin per 100ml DI water and 0 to 30g plasticizer (glycerol) per 100g gelatin were used for preparing different gelatin substrates and finding the best sensor coating that was structurally robust yet had a signal response in an hour time frame for these studies. To make the gelatin substrate, DI water was preheated to 72°C using a water bath on a hot plate. Granular gelatin procured from Carolina was added to the water and gently stirred using a stir bar. When the bath's temperature raised to 80°C, glycerol was added and the mixture was stirred for 10 minutes (Fig 8).

The resonant sensor starting frequency and extent of signal modulation were affected by the surface area of substrate added. When an O-ring with a 12.5mm diameter was epoxied at the center of the 40mm resonator, the resulting center well surface area was found

to have a clear start resonant frequency and signal response in the desired 1-100MHz range. A 200µl of substrate solution was poured into the center of the O-ring and cured for two hours at room temperature. Afterward, a 7.56mm diameter hole was made at the center of the solidified gelatin substrate to serve as the enzyme addition well (Fig 9).

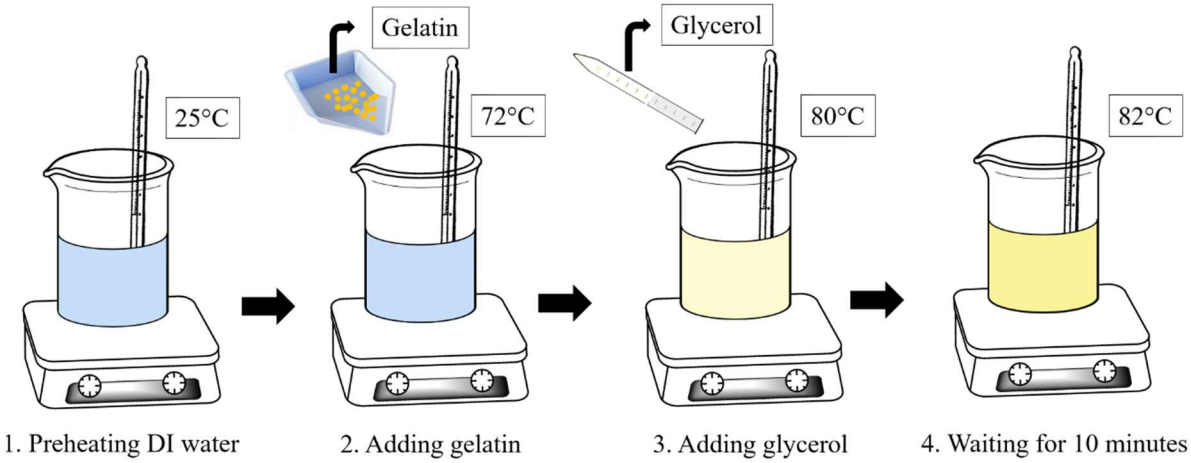

Figure 8 Preparation of gelatin substrate.

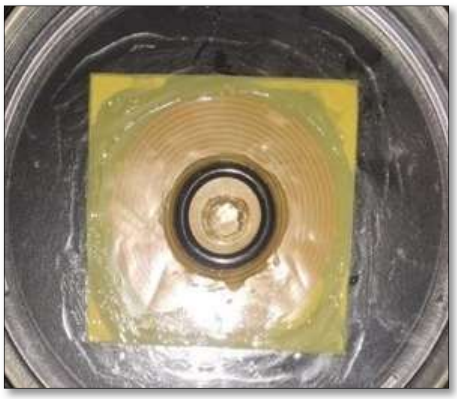

Figure 9 Substrate Coated resonator using an O-ring.

3.3.3 Bead Test for the Resonant Frequency and Radius Correlation

For the empirical relation of resonant frequency to radius measurement used to inform the transport model of the enzyme-gelatin system, 15µl of red fluorescent amine-modified polystyrene latex beads aqueous suspension was added to 15µl of 400mg/ml

solution of bacterial protease in PBS. This solution was poured into the gelatin hole and the webcam setup was used to take images of the degradation extent of every S_{21} data acquisition point (Fig 10).

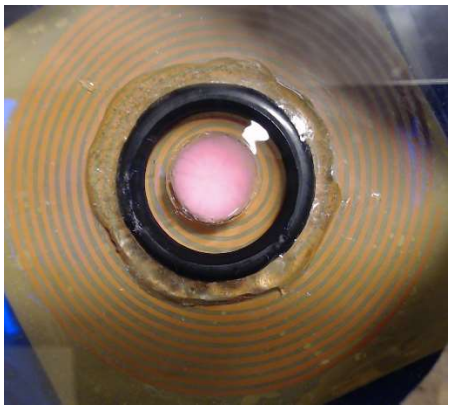

Figure 10 Pink fluorescent beads used for the empirical relation of resonant frequency to radius measurements.

3.3.4 Testing Substrate Coated Resonators

The petri dish was fixed above the reader coils at a 5mm displacement and the S_{21} magnitude (dB) versus the frequency (MHz) was collected every 15 seconds using automated Matlab scripts. After three minutes, 30µl of the enzyme solution was pipetted into the cut center well. The hydrogel degradation was monitored for three hours. The enzyme solutions used for these tests were prepared by dissolving 15 to 200mg of either bacterial protease or subtilisin A in 1ml phosphate-buffered saline (PBS) with a pH of 7.95. All tests in this study were conducted at room temperature.

3.3.5 Soil Tests

Soil samples (0-10 cm depth) were collected from a field near Boone, IA (41.920619 N, -93.750063 W). The soils were from the Nicollet and Webster soil series, Aquic Hapludoll, and Typic Endoaquoll respectively. The soils were brought back to the lab and

immediately stored at -80°C prior to testing. For these tests, the hydrogel was made using 7wt% gelatin and 20g glycerol/100g gelatin. 200µl of the gelatin solution was placed at the center of the epoxied O-ring on the standard resonator (D_o = 40mm, P = 1mm). After solidification, the gelatin was covered with parafilm and a 7.56mm diameter hole was made at the center of the gelatin and parafilm. After saving the background signal for two minutes, 1.1g of previously frozen loamy soil was premixed with 300µl DI water and placed in the center, sample hole. Wet paper towels were placed around the resonator in a petri dish to minimize evaporation over the course of the experiment.

CHAPTER 4. RESULTS AND DISCUSSION

4.1 influence of resonator geometry on the start resonant frequency

With initial prototyping, we found that prior resonant sensor designs that relied on a rigid closed loop circuit[72,73] or parallel plates folded together to complete a circuit[34], could be greatly simplified as an open circuit Archimedean coil. In this new design, the conductive spiral serves as the inductor and the narrow gaps between the conductive lines operate as the tuning capacitor. Resonators of varying lengths and pitch sizes were fabricated to determine the influence of resonator geometry on the start resonant frequency.

4.1.1 Length Effect

In order to study the effect of resonator length, multiple resonators with constant pitches of 1.2mm and different lengths (407-2764mm) were fabricated (Fig 11).

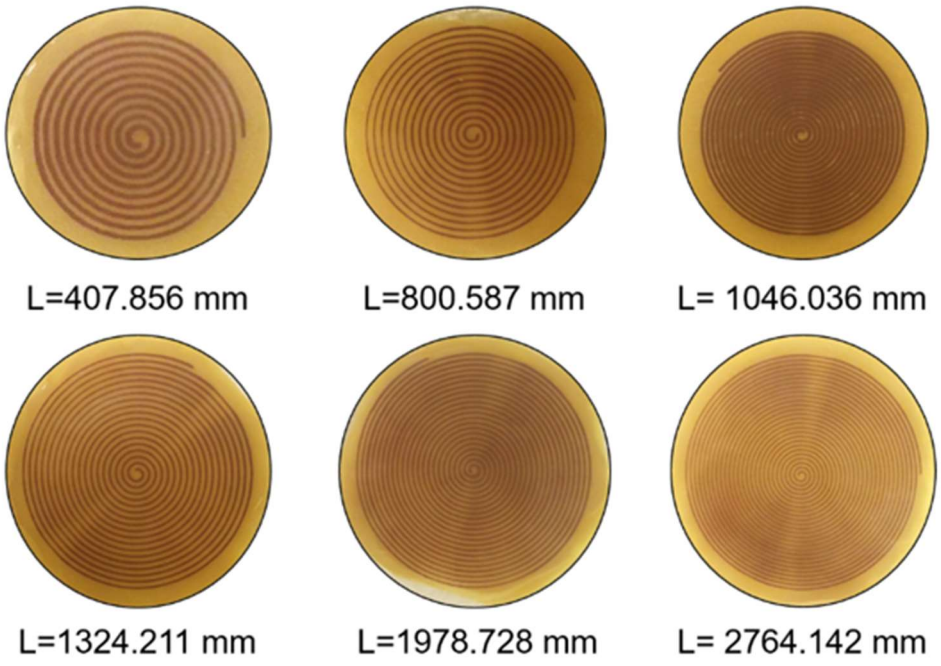

Figure 11 Constant pitch (1.2mm) resonant sensors with various lengths (407-2764mm).

It was observed that the resonant frequency of the resonators showed an inverse relationship with the length (Fig 12). A power function was used to fit the resonant frequency of the sensor vs length of the resonator (Fig 13).

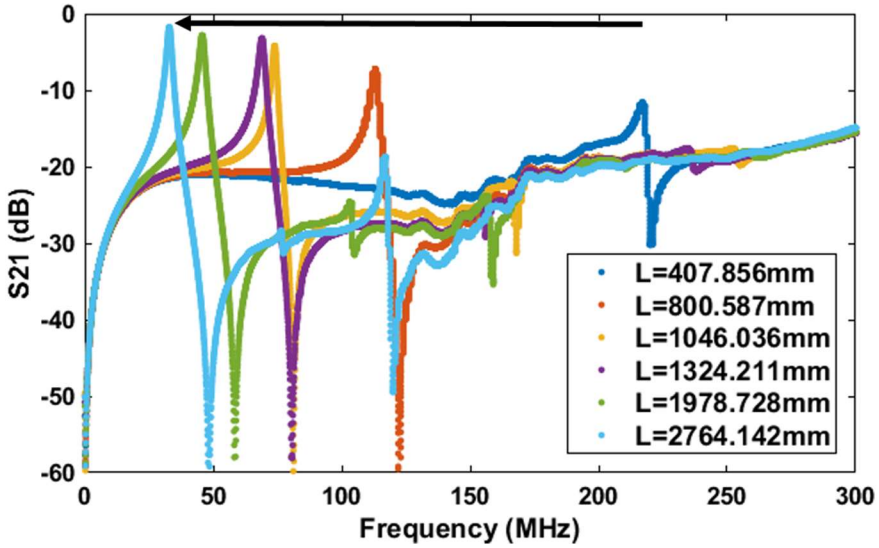

Figure 12 Effect of resonator length on the sensor response and the resonant frequency of the sensor

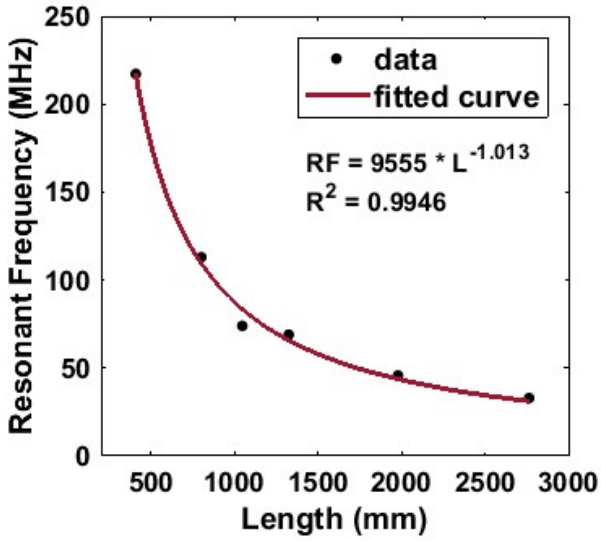

Figure 13 Power model fit on the experimental resonant frequency responses for different length sizes of the sensors.

4.1.2 Pitch Effect

For studying the effect of the pitch size, five resonators with a set length of 1255mm were designed with varying pitch sizes of 1, 1.2, 1.6, 2, and 2.5mm (Fig 14). It was observed that the resonant frequency of the resonator has a direct relationship with the pitch size (i.e. resonant frequency increased with increasing pitch size (Fig 15); however, it seems like the pitch size had a minor effect on the peak of the characteristic S_{21} magnitude sigmoidal response in comparison with the length size.

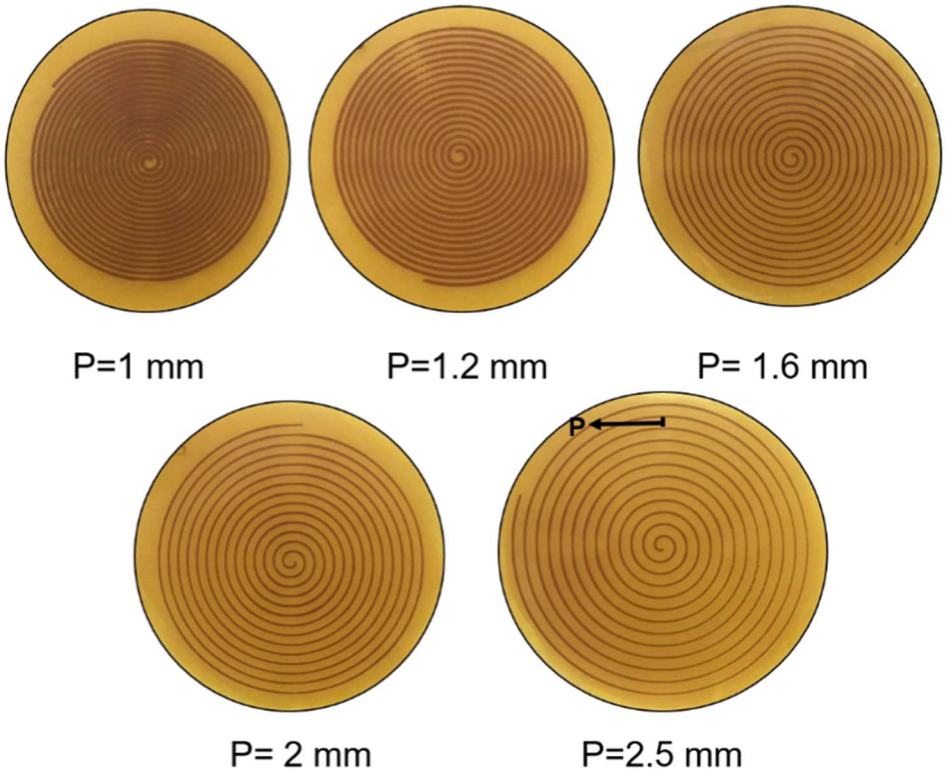

Figure 14 Fabricated resonant sensors with constant length (1255mm) and a pitch size range of 1-2.5mm.

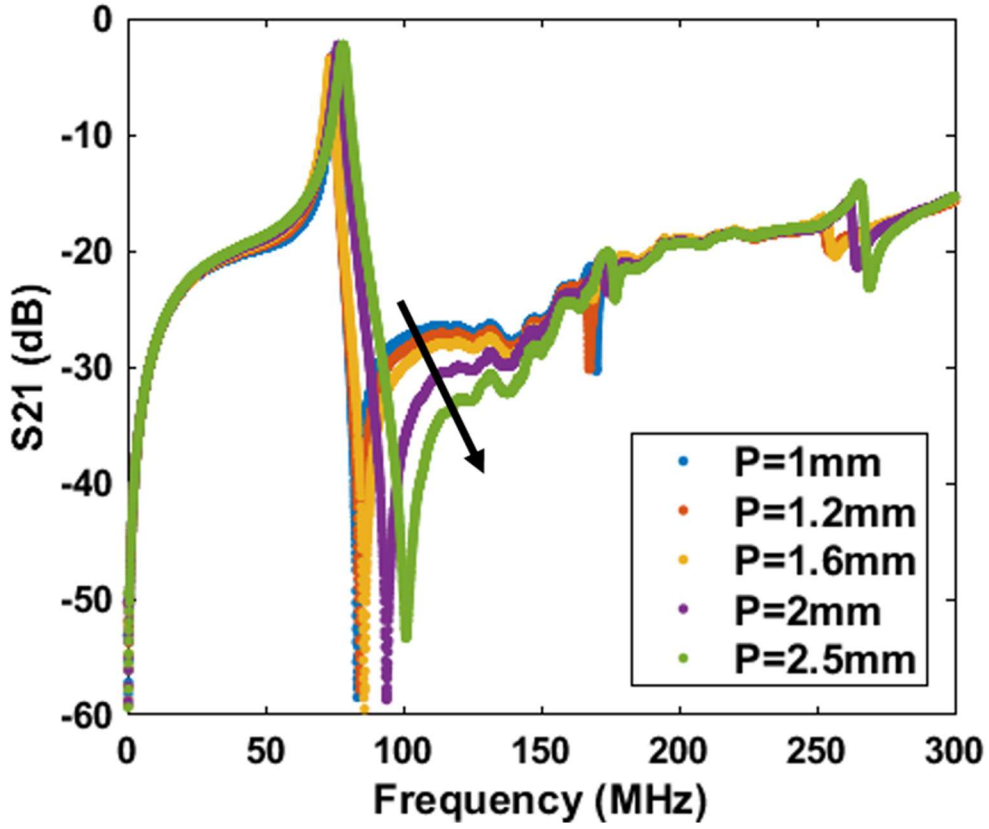

Figure 15 Effect of resonant sensor pitch size on the S_{21} magnitude response and the resonant frequency of the sensor.

The basic governing equation for the resonant frequency of an LC circuit with a parallel plate capacitor[74] is as follow:

$$Resonant\ Frequency = \frac{1}{2\pi\sqrt{\frac{L\,\varepsilon_r\,\varepsilon_0 A}{d}}} \tag{5}$$

Where L is the inductance, ε_r is the relative permittivity of the material, ε_0 is the permittivity of free space and (a constant equal to $8.854 \cdot 10^{-12}$ F/m), A is the capacitive area, and d is the capacitor plate displacement. Thus, the empirical observations of geometric effects on starting resonant frequency are physically grounded, as the increase in coil length results in an increased inductance and the increased pitch size decreases the capacitance.

4.2 Effect of Relative Permittivity on Resonant Frequency

The governing equation (Eq. 5) shows that the relative permittivity of the material near the inductive coils also has a direct effect on the resonant frequency. This was validated by observing the change in resonant frequency of a sensor going from an air relative permittivity ($\varepsilon_r \approx 1$), to placing water ($\varepsilon_r \approx 80$ at 20°C) on the sensor surface and then replacing the water with oil ($\varepsilon_r \approx 3$ at 20°C). Each caused an expected shift based on the change in the dielectric (Figure 16).

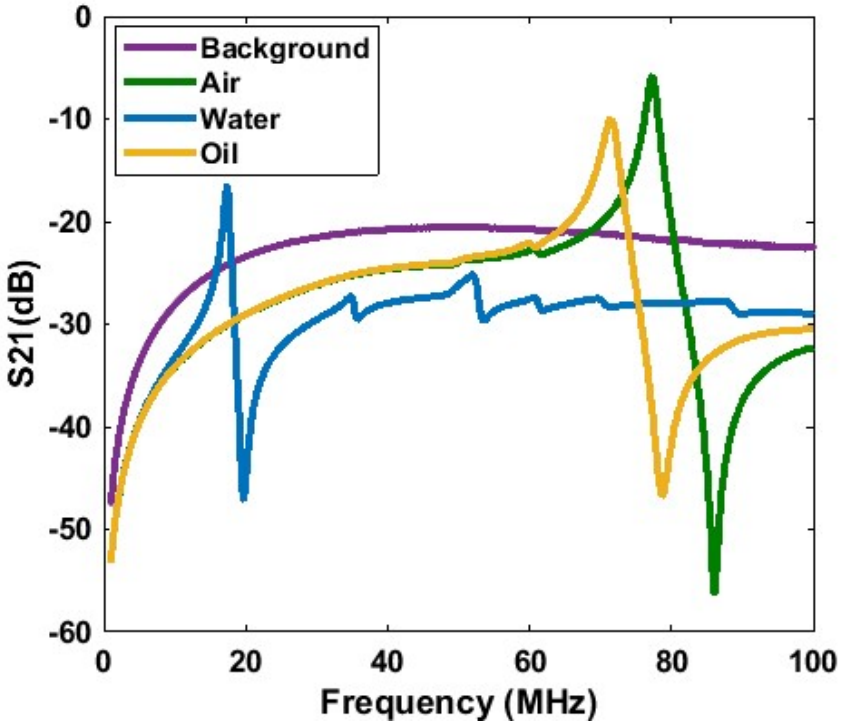

Figure 16 Resonant sensor response (S_{21} magnitude) for materials with different relative permittivity.

Since the resonant frequency is inversely proportional to the permittivity, the resonant frequency of air started at a higher frequency in comparison with a high-dielectric medium of water. For a medium with intermediate permittivity (vegetable oil), the resonant frequency was between the water and air. Furthermore, we determined that the resonant

sensor was responsive to the amount of liquid present on the surface, by adding increasing amounts of deionized (DI) water and vegetable oil (0 to 4.5ml). Unsurprisingly, the change in resonant frequency for adding high relative permittivity water was 60 MHz while this shift was about 4MHz for the same volume of oil (Figure 17).

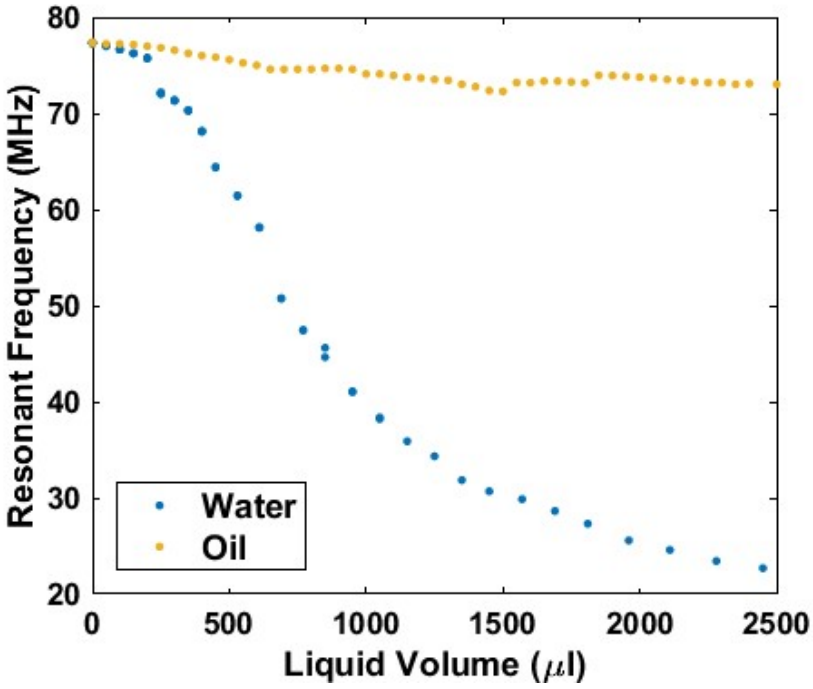

Figure 17 Comparison of the resonant frequency changes of the standard resonator having deionized water vs vegetable oil on the resonator's surface.

4.3 Design of Hydrolytic Enzyme Activity Measurement Tests

With this fundamental understanding of resonator frequency tuning and response to a change in the surface dielectric, we then designed a sensor that would transduce the activity of hydrolytic enzymes. By coating the polyimide surface with the target substrate of the enzyme, the resonator has a defined starting frequency; as the enzyme degrades the substrate, the change in the surface dielectric is then transduced via a change in the resonant frequency (much the same as shifting from oil to water as above). After a few design iterations, we determined the optimal amount of substrate to place at the center of the resonator to allow for

a full response window in the 1-100MHz range. This high, very high-frequency range was targeted for its ability to penetrate aqueous, tissue, and plastic systems.[75,76]

To improve reproducibility of the tests, we secured an O-ring (12mm Inner Diameter) to the center of the resonator in which the enzyme substrate could be drop cast (Fig 18-I). For the tests in this paper, the substrate was gelatin and the hydrolytic enzymes were various proteases. The gelatin would set (Fig 18-II) and a punch was used to remove a 4mm diameter section of gel (Fig 18-III) to create a test well to insert the enzyme (Fig 18-IV). The resonator was then placed on a two loop antenna reader in order to study the substrate degradation process (Fig 18-V and VI).

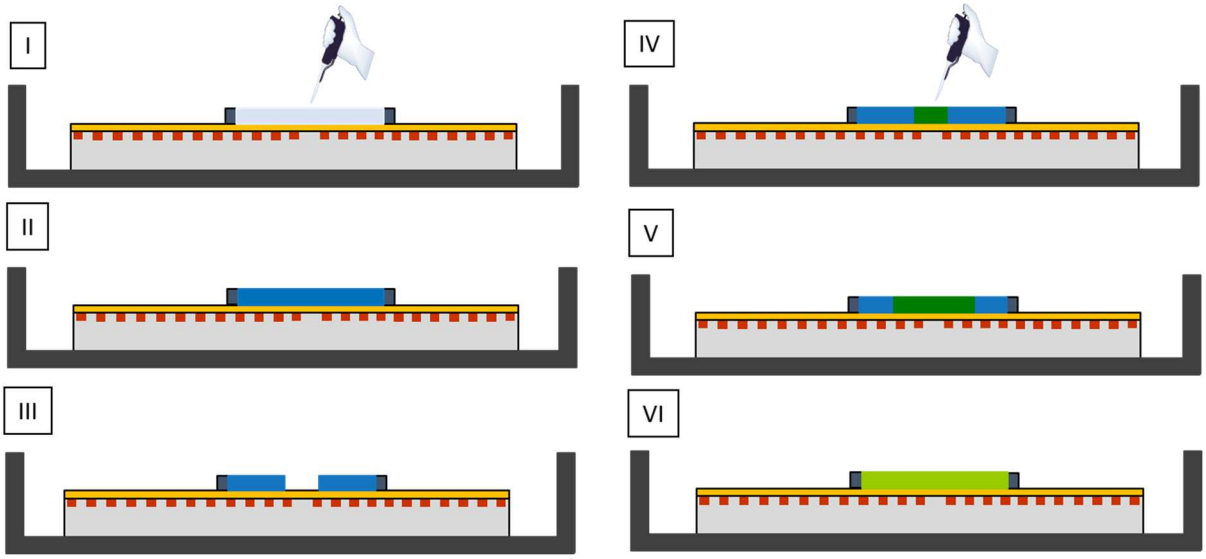

Figure 18 Design of the substrate-coated resonant sensor for hydrolytic enzyme activity and the digestion of the substrate.

The resonator S_{21} magnitude scattering parameter is observed in Figure 19 for three different stages:

1. Solidified gelatin substrate containing a punch out center for inserting the enzyme sample

2. Gelatin substrate and 30µl enzyme solution right after addition of enzyme

3. Digested gelatin

As mentioned before, the resonant frequency is defined as the peak of the sigmoidal S_{21} curve.

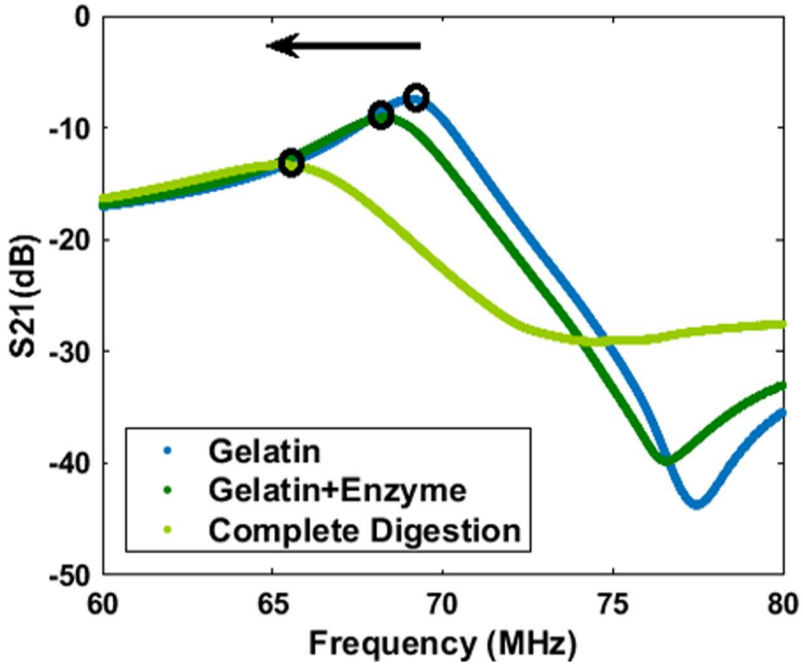

Figure 19 S_{21} magnitude response curves for gelatin, gelatin with enzyme, and gelatin after digestion.

The effect of enzyme concentration on the resonant sensor response was studied for two proteases:

1. purified Subtilisin A with a defined hydrolytic activity provided by the vendor

2. unpurified bacterial protease with unknown activity

4.3.1 Purified Subtilisin A Test

The resonant sensor response was monitored for different concentrations of Subtilisin A. The gelatin substrate composition for these tests was 14 wt% gelatin and 20g glycerol/100g gelatin. Subtilisin A was tested at concentrations of 30, 70, and 200 mg/ml. The S_{21} magnitude from 1 to 100MHz was recorded for three hours after enzyme addition. The peak of the resonant sensor sigmoidal curve was then plotted as a function of time (Fig 20). As expected the resonant frequency decreased for all enzyme concentrations. For all traces there was a large, initial decrement in resonant frequency due to the addition of liquid (high relative permittivity) to the dry resonator; however, after this initial jump, the rate of change was dependent on enzyme concentration, with the higher enzyme concentrations leading to lower resonant frequencies due to a larger extent of digestion. As the gelatin degrades, there is a dielectric shift which we attribute to more water access on the resonator surface which causes the resonant frequency decrease.

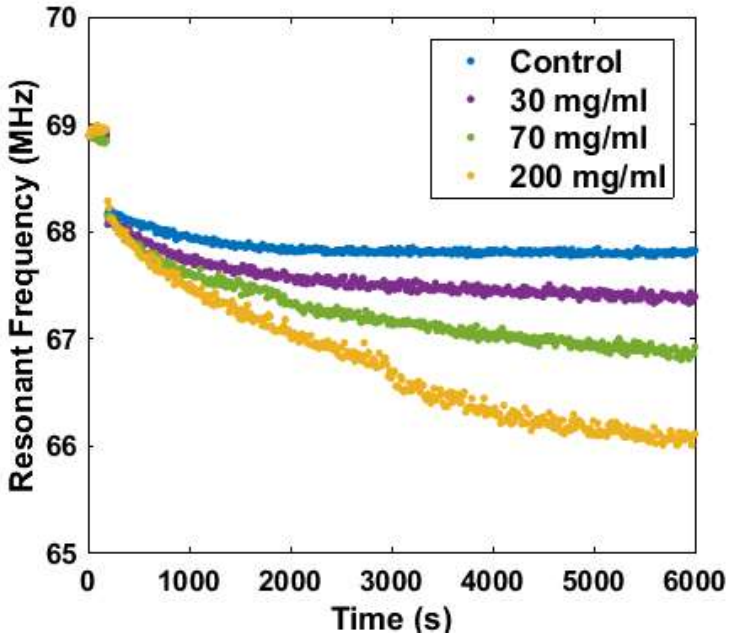

Figure 20 Resonant sensor response for different concentrations of Subtilisin A.

4.3.2 Unpurified Bacterial Protease Test

The test performed for the unpurified bacterial protease was the same as the test for Subtilisin A. The S_{21} magnitude was monitored for three hours after addition of 15,30,70, and 200mg/ml enzyme solution and the resonant frequency was plotted as a function of time (Fig 21). The response followed the similar trend as the Subtilisin A in terms of the initial drop of the resonant frequency and the general effect of enzyme concentration on the resonant frequency (higher enzyme concentration leads to a lower resonant frequency); however, it was observed that the shift of the resonant frequency was larger for the unpurified bacterial protease than the shift for the purified Subtilisin A. This observation led to the assumption that the hydrolytic activity (k_{cat}) is higher for the bacterial protease in comparison with the Subtilisin A.

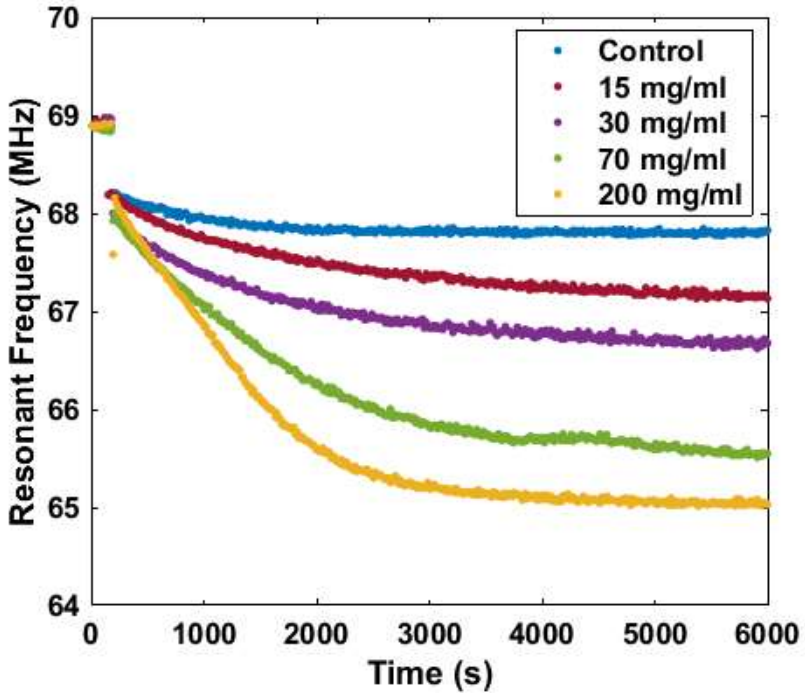

Figure 21 Effect of bacterial protease concentration on the resonant frequency response of the sensor.

4.4 Modeling

The enzymatic degradation process of hydrogel was modeled for different enzyme concentrations and hydrogel compositions in order to fit the sensor's frequency response data traces. The geometry of the model (Fig 22) shows that the mass conservation equation for the cylindrical coordinate (Eq. 6) can be used at this mass transport and reaction problem:[77]

$$\frac{\delta C}{\delta t}+v_r\frac{\delta C}{\delta r}+\frac{v_\theta}{r}\frac{\delta C}{\delta \theta}+v_z\frac{\delta C}{\delta z}=D\left[\frac{1}{r}\frac{\delta}{\delta r}\left(r\frac{\delta C}{\delta r}\right)+\frac{1}{r^2}\frac{\delta^2 C}{\delta \theta^2}+\frac{\delta^2 C}{\delta z^2}\right]+R_v \tag{6}$$

Where C is the concentration of enzyme in the system, v is the transport velocity, D is the diffusion coefficient of the enzyme through the substrate (gelatin hydrogel), R is the rate of enzyme reduction, and r, θ, and z are radial, angular, and height dimensions. For simplification, two assumptions can be made at this stage:

1. the total enzyme concentration in the system is constant (R = 0, no depletion)

2. the transport toward angular (θ) and height (z) dimensions are neglected.

Therefore, the problem is simplified to a singular radial dimension and the following partial differential equation (PDE) can be obtained (Eq. 7):

$$\frac{\partial C}{\partial t}=D\left[\frac{1}{r}\frac{\delta}{\delta r}\left(r\frac{\delta C}{\delta r}\right)\right] \tag{7}$$

There are two spatial and one initial boundary conditions for this PDE:

1. at time zero, the enzyme concentration throughout the entire substrate gel is zero

2. at all times the flux at the O-ring interface ($r = R_b$ in Fig 22) is zero

3. the concentration of enzyme at the reactive interface ($R_i(t)$ in Fig 22) is equal to the concentration of enzyme in the center well.

The third boundary condition is actually a Stefan boundary condition. The Stefan problem is known as one of the simple mathematical models for phase change phenomena. The feature of this boundary condition which makes it different from the other two is that the location (R_i) is time-dependent itself. As the gel digests during the experiment, the reactive interface (R_i) increases and moves towards the O-ring.[78–80] This boundary condition is further complicated since the center well enzyme concentration is not constant and the diffusion of the enzyme into the hydrogel results in a decrement in the enzyme concentration. Since these type of transport problem cannot be solved analytically, numerical methods were used for modeling purposes. Centered finite differences in the spatial domain with a grid resolution of 10µm and 4th order Runge Kutta solver (Matlab ode45) in the time domain were applied for numerical modeling (Appendix A.3).

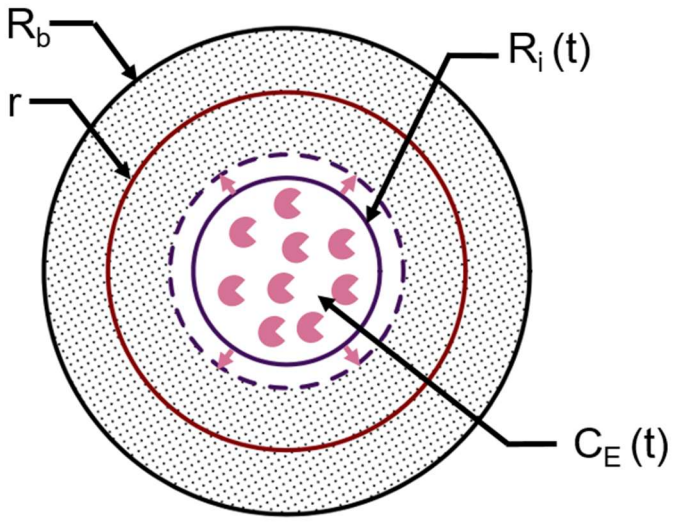

Figure 22 Simplified mass balance problem by reducing the problem to radial coordinates.

As the initial step for the numerical solution, the above-mentioned governing PDE is written in finite difference form:

$$\frac{\partial C}{\partial t} = D\left[\frac{1}{r}\frac{\delta}{\delta r}\left(r\frac{\delta C}{\delta r}\right)\right] = D\left[\frac{\delta^2 C}{\delta r^2} + \frac{1}{r}\frac{\delta C}{\delta r}\right] \tag{8}$$

The following general finite difference approximations can be used for the above-mentioned PDE:

$$\frac{\delta C}{\delta r} = \frac{C_{i+1,j} - C_{i-1,j}}{\Delta r} \tag{9}$$

$$\frac{\delta^2 C}{\delta r^2} = \frac{C_{i+1,j} - 2C_{i,j} + C_{i-1,j}}{\Delta r^2} \tag{10}$$

Therefore, centered finite difference form of the PDE with $O(h^2)$:[81]

$$\frac{C_{i,j+1} - C_{i,j}}{\Delta t} = \frac{D}{r_i \Delta r^2}\left(r_{i+\frac{1}{2}} C_{i+1,j} - 2r_i C_{i,j} + r_{i-\frac{1}{2}} C_{i-1,j}\right) \tag{11}$$

In which r_i is the radial point and i = 1, 2, 3….N represent the node positions of the mesh, $r_{i\pm1/2}$ are halfway positions between the nodes, Δr is the mesh spacing which is equal to 10 μm and j is the time step index. The center of the cylinder is denoted as $r_1 = 0$.

Defined forms of the finite difference equation at the endpoints are used for managing the boundary conditions mentioned earlier. The simulation time is slowly stepped forward and the extent of the substrate (hydrogel) digestion is determined in each of the volumetric shells. These volumetric shells are defined by the nodes used for controlling the Stephan boundary condition. The node is effectively removed in case of having complete digestion.

Afterward, the finite differences jump to the following furthest node on the subsequent start time. In order to provide the solution vector of the position of the reactive front (R_i) *vs.* time, the time points of these digestion events are recorded.

Although the developed transport model was successfully fitted to all of the empirical data, it has some limitations which cannot be neglected. For instance, the response curve is simplified because of applying the mesh approach for the spatial domain. There is a gradual change in the diffusion coefficient at the interface in a real digestion problem rather than sharp disjointedness among the nodes.

There were no significant abnormalities observed for the medium to high enzyme concentration model fit; however, there was an initial lag time for the digestion of the first node at low enzyme concentrations as the gel is loaded by diffusing enzyme. This lag time was ascribed as an artifact of the mesh spacing approach, therefore was neglected, and the time at which the first layer of gel was digested was stated as initial test time (t=0). After the simulation of the following digestion patterns (subsequent layers), the transport model was fitted to the empirical R_i vs time curves. In order to improve the above-mentioned complexities by reducing the simulation time, an adaptive grid (*e.g.* one that has close spacing near the reactive boundary, and gets coarser grained in the bulk gel) could be used; however, we feel this is beyond the scope of the current research project.

4.4.1 Bead Test for Modeling

In order to have a numerical model for the substrate degradation, the correlation of frequency response of the resonant sensor and the change in the reactive interface radius (R_i) is required. This was determined empirically by recording the motion of dyed polystyrene

beads as the gel digests (Fig 23). The test was run for 12000s and the sensor response, as well as an image of the O-ring area, were collected each 20s.

Using the code for bead image analysis (Appendix A.4), the upper left and the lower right of the O-ring were selected in order to have the program zoomed into the O-ring region as the initial step. Next, four interior points of the O-ring were selected so that the program could find the center and the diameter of the O-ring in pixel. In the last step, three spots at reaction front of the gel were selected for every 600 pictures, in order to record the inner radius (R_i) in pixels. Knowing the real inner diameter of the O-ring and the diameter in pixel, the radius in pixel can be converted to mm for all of the data points.

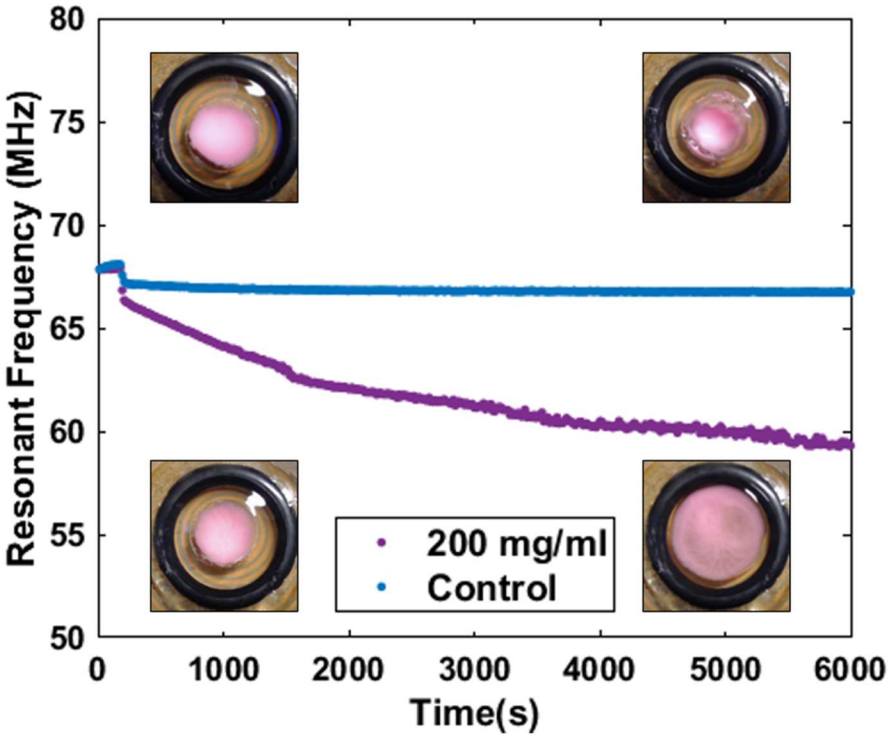

Figure 23 Change in resonant frequency during digestion with tracker beads in the center well (inserts show screenshots from video of the control sample and digested sample).

The resonant frequency was converted to the reactive front radius as a function of time using Matlab image processing (Fig 24–Appendix A.4). The quadratic fit for the captured inner radius data over 12000s is as follow:

$$R_i(t) = -1.111*10^{-8}*t^2 + 0.0002986*t + 3.997 \quad (12)$$

The R-squared for such fit is equal to 0.9613.

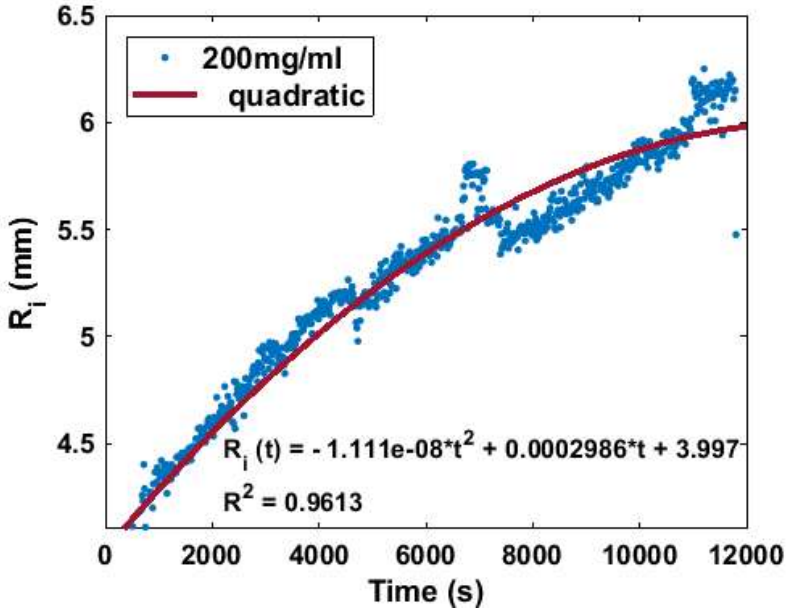

Figure 24 Reactive front radius vs. time data extracted from digested bead video with accompanying quadratic fit.

The frequency drop of the sensor can be expressed as a function of the reactive radius location (Fig 25). The quadratic fit with $R^2 = 0.977$ is shown in Equation 11:

$$\Delta F = -1.4857*R_i^2 + 17.899*R_i - 46.444 \quad (13)$$

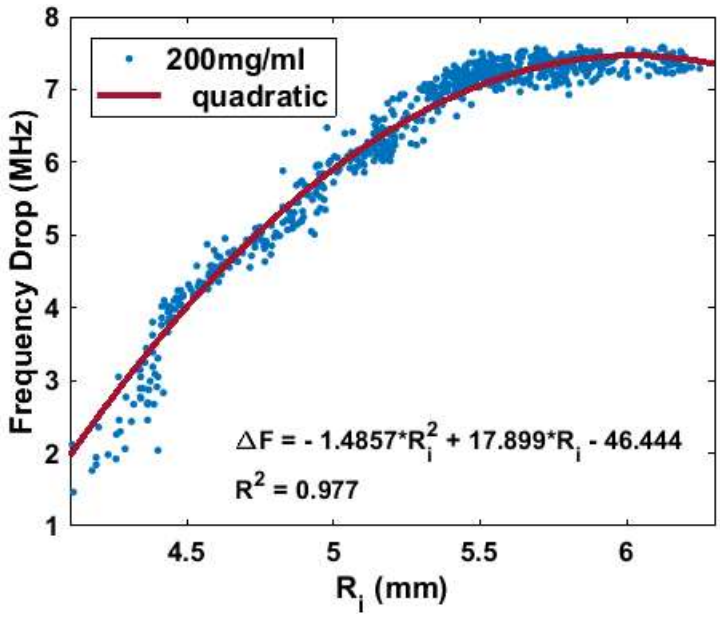

Figure 25 Relation of frequency drop to the reactive front radius.

The model's radial response trajectories are dependent on the enzyme start concentration (Fig 26), turnover rate (Fig 27), and the diffusion constant which is set at 10^{-6} cm^2/s for these figures.

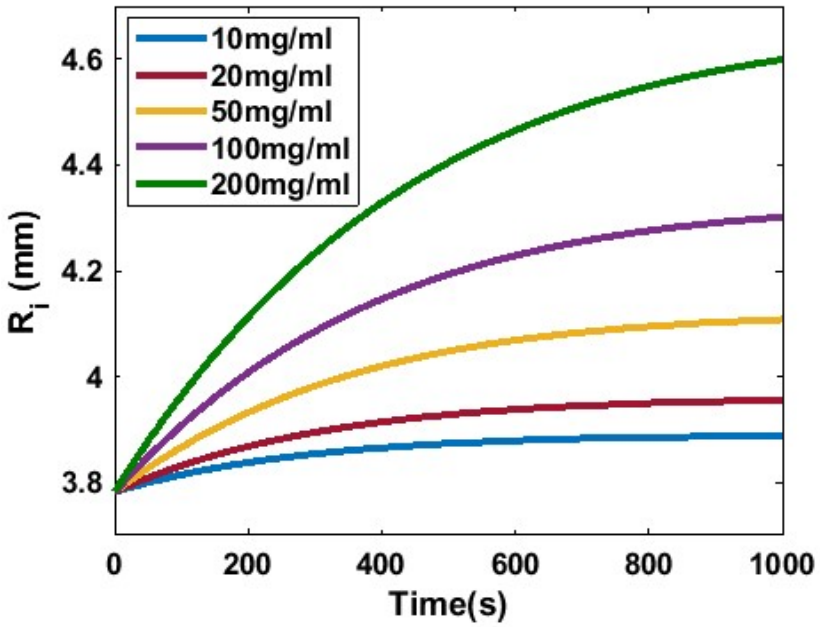

Figure 26 Digest model simulations at various enzyme concentrations for 1000s.

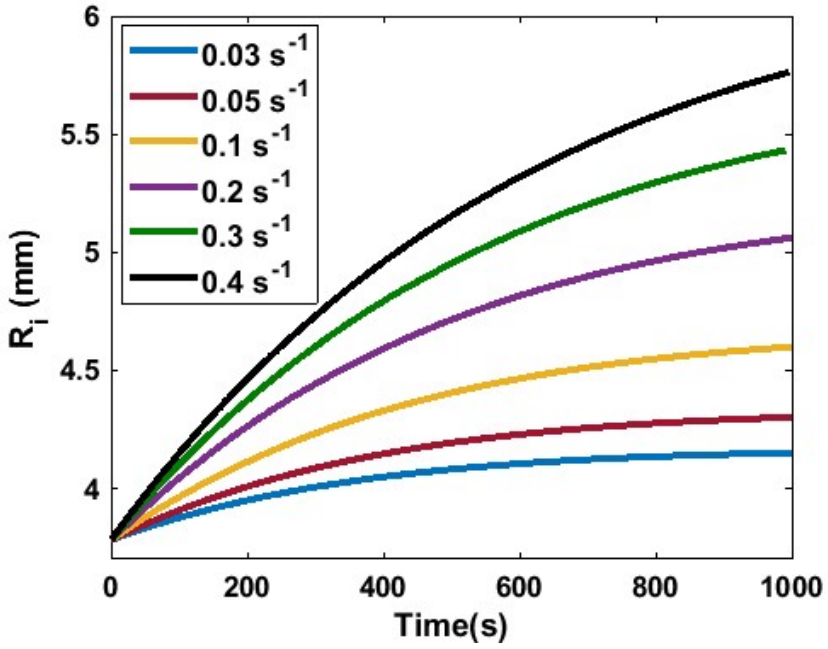

Figure 27 Developed digest model for different enzyme turnover rates.

4.4.2 Transport Model for Subtilisin A

Applying the above-mentioned empirical relation between change in the resonant frequency and R_i (Eq. 11), the collected data for Subtilisin A in terms of the resonant frequency as a function of time can be converted to the position of the reactive front (R_i) vs. time (Fig 28). Afterward, the transport model can be used for governing the k_{cat} value for which the best fit for the experimental data could be obtained (Fig 29 and Table 3). The model fit was limited to the first 1000s time points because of the simulation time restrictions since it almost takes 10 minutes for each simulation which should be iterated many times to converge on the best k_{cat} value.

For the diffusion constant we found literature values ranging from $1.017 \cdot 10^{-6}$ to $2.46 \cdot 10^{-6}$ cm^2/s in water[82–84] and from $4 \cdot 10^{-8}$ to $5 \cdot 10^{-7}$ cm^2/s in hydrogel (which is approximately 10 to 100 times lower in comparison with the diffusion coefficient in water)[85] and decided to fix our model at $1.7 \cdot 10^{-7}$ cm^2/s based on goodness of fit to our data. Since the

k_{cat} of an enzyme is an intrinsic property (a fundamental property which is independent of any factor such as the amount of material)[86], it should be conserved through the different enzyme concentrations; however, small variations in the turnover rate value for different enzyme concentrations were observed. This could be due to the experimental variance, but it could also be due to the increment in the amount of enzyme present in a solution which acts as a competitive substrate. In other words, at higher enzyme concentrations, some of the enzymes will digest other enzymes rather than the substrate which would result in a reduction in the observed k_{cat} value.

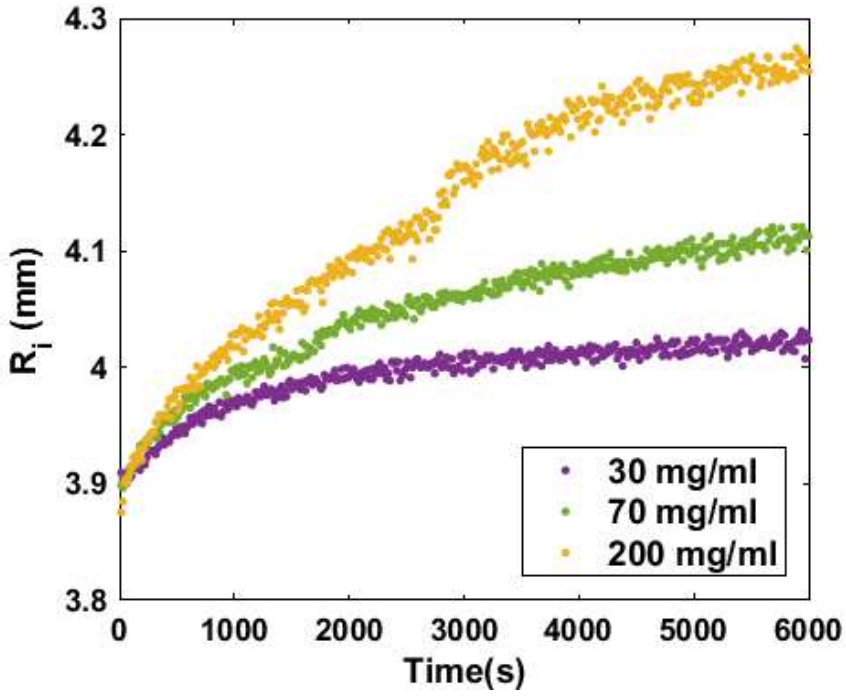

Figure 28 The changes in enzyme well radius corresponding to experimental data for purified Subtilisin A.

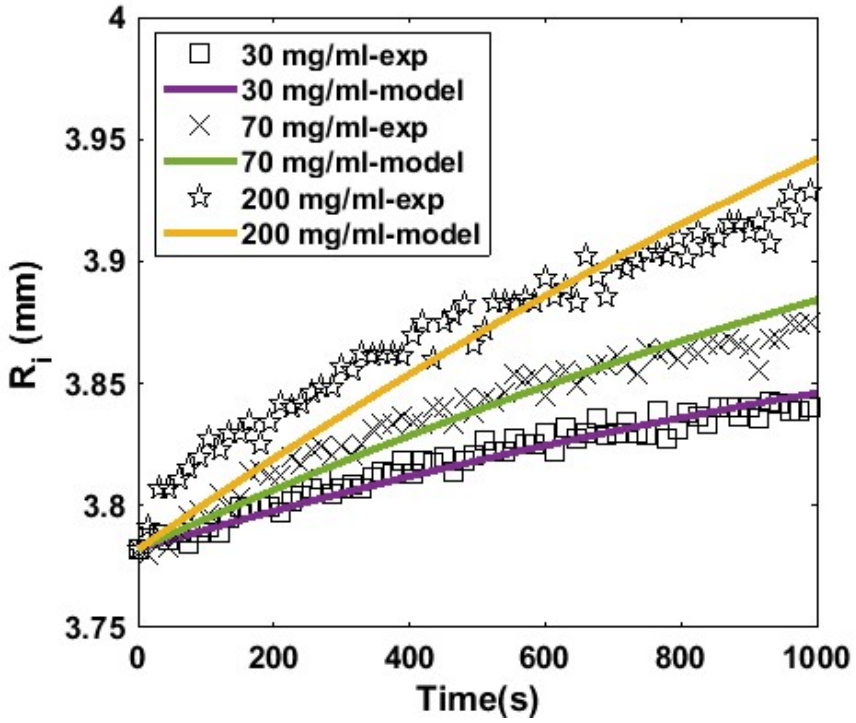

Figure 29 The model fit on the first 1000(s) of the experimental data for Subtilisin A.

Table 3 K_{cat} values for different concentrations of Subtilisin A.

Concentration (mg/ml)	30	70	200
K_{cat} (s^{-1})	0.003	0.00275	0.00205

It is difficult to compare the k_{cat} measurements using the resonant sensors to the reported literature values for the enzyme activity due to the fact that the activity is usually defined with activity units which are relative measures to another protease or known substrate analog. For instance, the Subtilisin A used in our experiments has a specified activity provided by the vendor (Sigma) equal to 7-15 units/mg solid. The unit is defined by Sigma as hydrolysis of casein at pH equal to 7.5 and temperature equal to 37°C for producing color corresponding to 1.0 µmole which is equal to 181µg of tyrosine per minute (color by

Folin-Ciocalteu reagent). Assuming 7units/mg activity, the activity of Subtilisin A which is provided by the vendor is equal to 0.0211 s^{-1} on a gram tyrosine per gram enzyme basis.:

$$activity = 7\frac{\text{units}}{\text{mg enzyme}} * \frac{181\mu\text{g substrate}}{\frac{1\text{ min}}{1\text{ unit}}} * \frac{1\text{g substrate}}{1000\mu\text{g substrate}} * \frac{1\text{ min}}{60\text{ sec}} = 0.02111/\text{s}$$

This value is roughly comparable to the k_{cat} values obtained from the resonant sensor response using the model fit considering the fact that the experiments here were conducted at 20°C which is lower than the temperature in which the vendor activity is provided (37°C). Moreover, the activity provided by the vendor is with regards to a different substrate (tyrosine) while we are measuring with reference to the start gelatin mass. The reason that we think the substrate basis k_{cat} reported in this thesis is more useful catalytic measure than the activity reported by the vendor is that the activity reported by the vendor is based on only one of the many byproducts of digestion. Hydrolysis of tyrosine cannot be a representative of the degradation of an actual substrate of interest while in our method we can easily report the activity based on the full digestion of any material (substrate) coated on the resonator.

4.4.3 Transport Model for Bacterial Protease

The resonant frequency vs. time data collected for different concentrations of unpurified bacterial protease was converted to R_i as a function of time (Fig 30). As expected, the changes in R_i are also larger for different concentrations of bacterial protease in comparison with Subtilisin A.

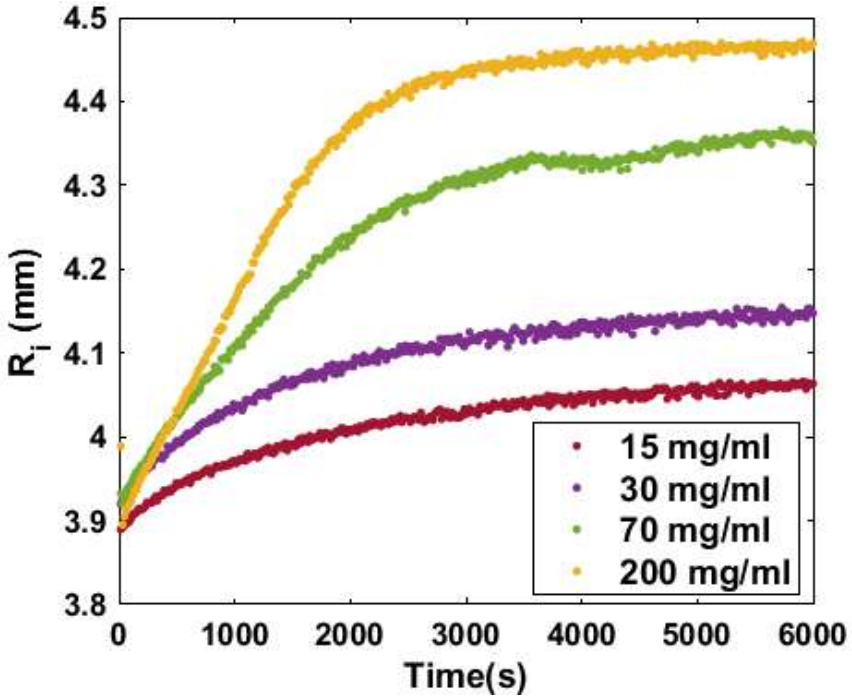

Figure 30 The changes in enzyme well radius corresponding to experimental data for the unpurified bacterial protease.

The k_{cat} values for the transport reaction model fit using a diffusion constant equal to $1.7 \cdot 10^{-7}$ cm^2/s on the experimental data corresponding to the bacterial protease test can be seen in Table 4 and Figure 31.

Table 4 K_{cat} values for different concentrations of unpurified bacterial protease.

Concentration (mg/ml)	15	30	70	200
K_{cat} (s^{-1})	0.009	0.008	0.0065	0.0037

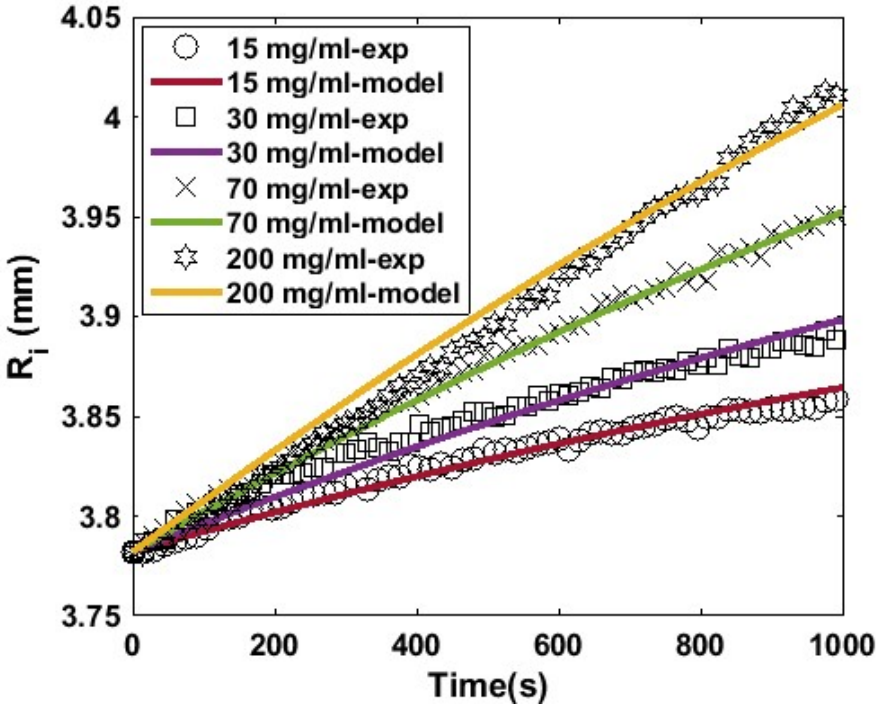

Figure 31 Transport model fit for different concentrations of unpurified bacterial protease.

Comparing the obtained k_{cat} values for Subtilisin A and bacterial protease (Table 3 and Table 4), it can be concluded that the assumption of higher hydrolytic activity for a bacterial protease is true.

4.5 Effect of Hydrogel Composition on Sensor Response

In order to study the effects of hydrogel composition on the sensor response, substrates with different gelatin and glycerol concentrations were made and tested with 200mg/ml bacterial protease solution. Hydrogels containing 7, 10, and 14 wt% gelatin with constant plasticizer concentration (20g glycerol/100g gelatin) were measured. The drop in resonant frequency showed an inverse relationship with the gelatin concentration (Fig 32).

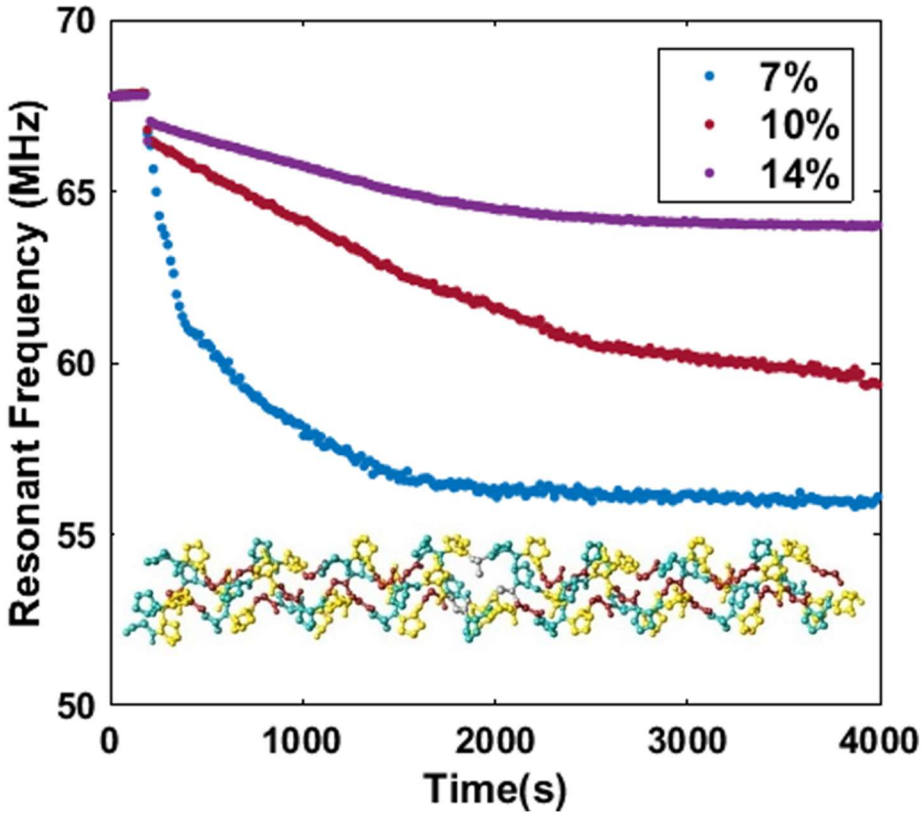

Figure 32 Effect of gelatin wt% on sensor response trajectory, gelatin structure is shown as insert.

The digestion model was run at these higher gelatin concentrations in order to predict the enzyme activity for these data (Fig 33) and resulted in k_{cat} fit values of 0.13, 0.014, and 0.0037 s^{-1} for 7, 10, and 14 wt% gelatin respectively. To get best fit for 7 wt% gelatin, we had to increase the diffusion constant to 10^{-6} cm^2/s, which is physically reasonable as a decreasing amount of gelatin would have larger pore sizes and an increased diffusion constant. We hypothesize that the observed decrease in k_{cat} as the gelatin concentration increases is a real effect due to different structural morphologies of the gelatin (more entangled structures at higher concentrations *vs.* easier to digest, sparse structures at lower concentrations).

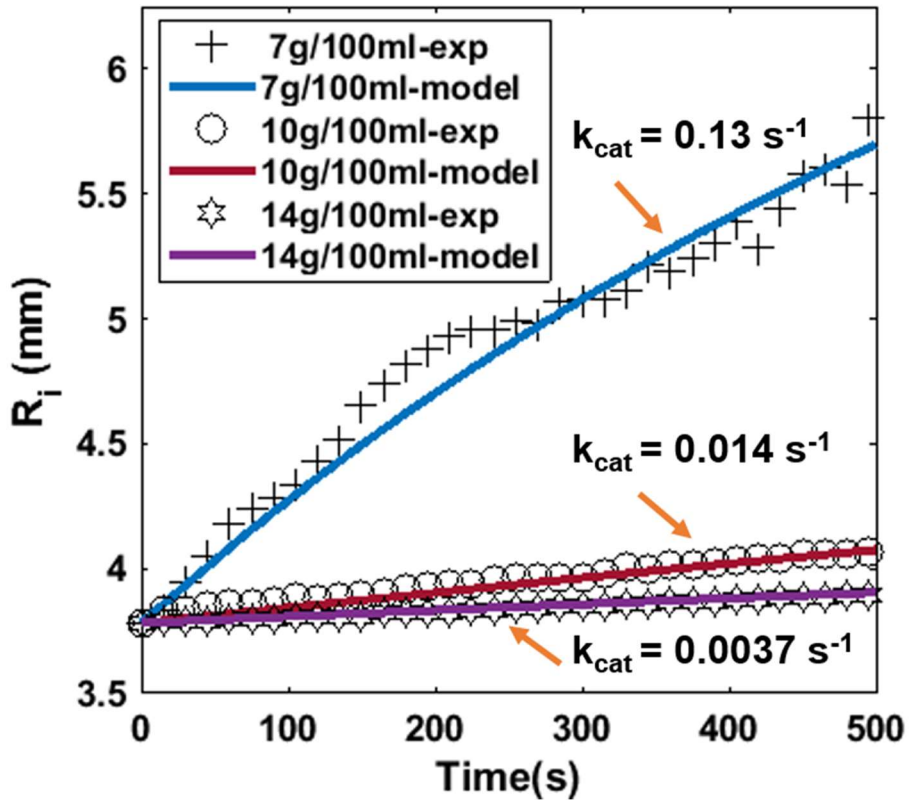

Figure 33 Model fit for different gelatin concentrations.

For studying the effect of plasticizer, 20, 30, and 40g glycerol/100g gelatin were used in a 14wt% gelatin hydrogel. It was seen that higher plasticizer concentration led to a lower resonant frequency (Fig 34). We attribute this due to a higher swelling ratio, allowing for more diffusion of the enzyme, and thus greater rate of digestion. In effect, these experiments demonstrate the tunability of the sensor response; the response rate and signal duration can be tuned for target enzyme concentrations based on substrate composition.

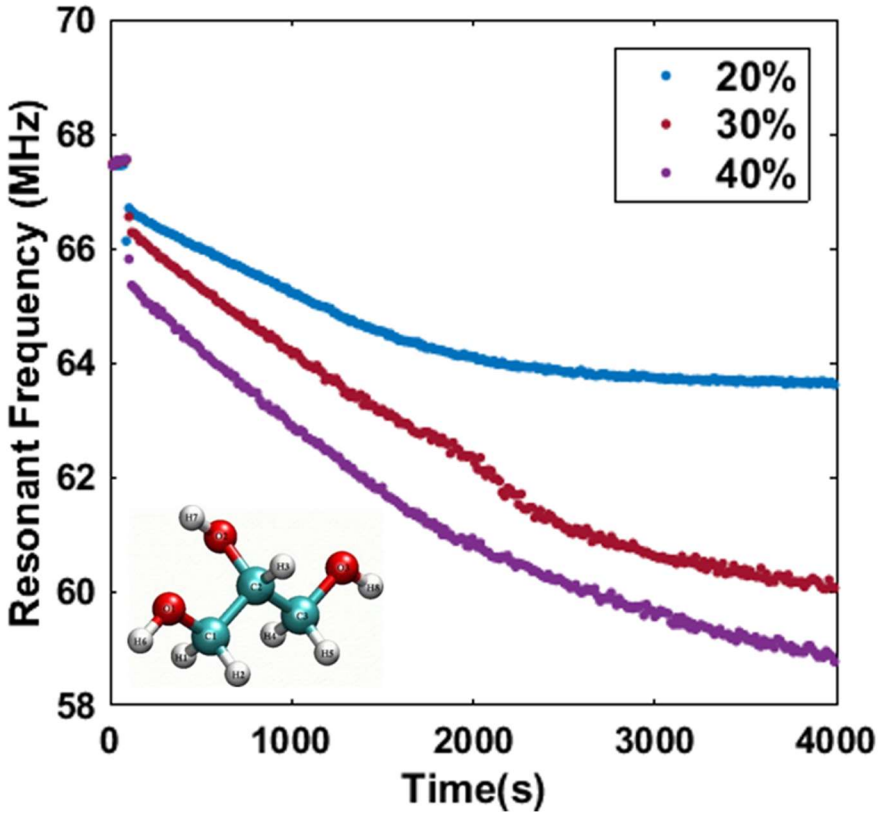

Figure 34 Plasticizer wt% effect on sensor response.

4.6 Soil Test

To test the capability of the resonant-based sensor for contact-free, *in situ* soil enzyme activity measurement, soil samples from the Iowa State Century Farm were tested. About 8.6MHz decrement in resonant frequency was observed after an hour for the soil sample. To create a control test, the soil sample was autoclaved at 120°C and the same experiment was repeated. There was no significant shift in resonant frequency after the control soil addition (Fig 35). To simulate soil with increased enzyme activity, a sample was spiked with 30µl of 200mg/ml bacterial protease and the same experimental procedure was conducted which resulted in 16MHz resonant frequency shift.

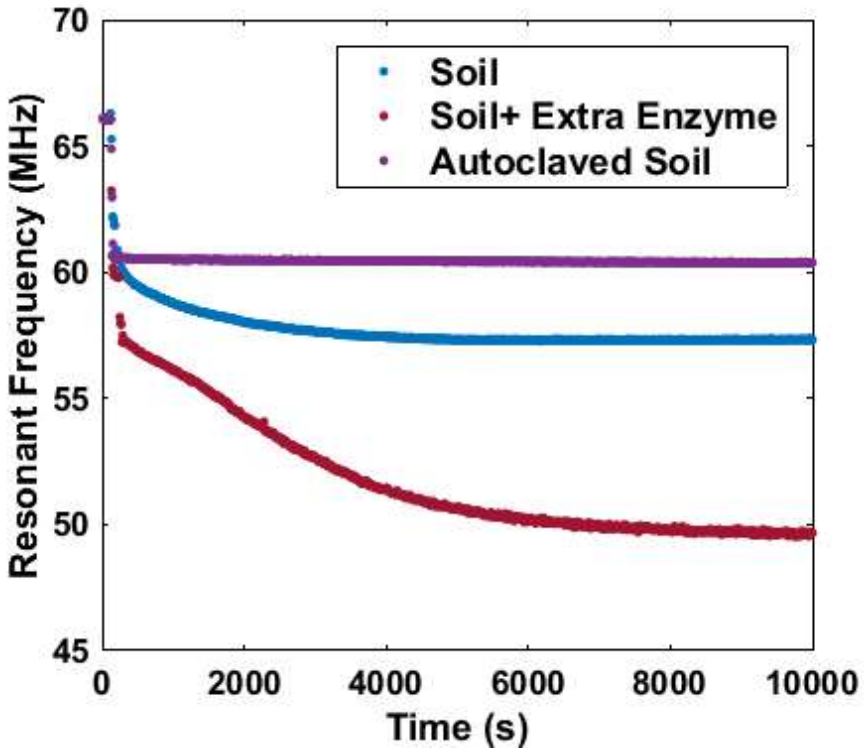

Figure 35 The sensor response for autoclaved soil, regular soil, and soil with the added enzyme.

The soil data was fit with the digestion model and resulted in a k_{cat} = 0.119 $g_{substrate}/(g_{enzyme} \cdot s)$ at an assumed enzyme concentration of 19.2 mg/ml. Because the concentration is not known, it is better to use the density of the soil (1.498 g/ cm^3 in this experiment, which falls in literature range[87] of 0.1-1.5 g/cm^3) and transform the activity to a soil mass basis; for this experiment we find a k_{cat} of 0.00152 $g_{substrate}/(g_{soil} \cdot s)$ (Fig 36).

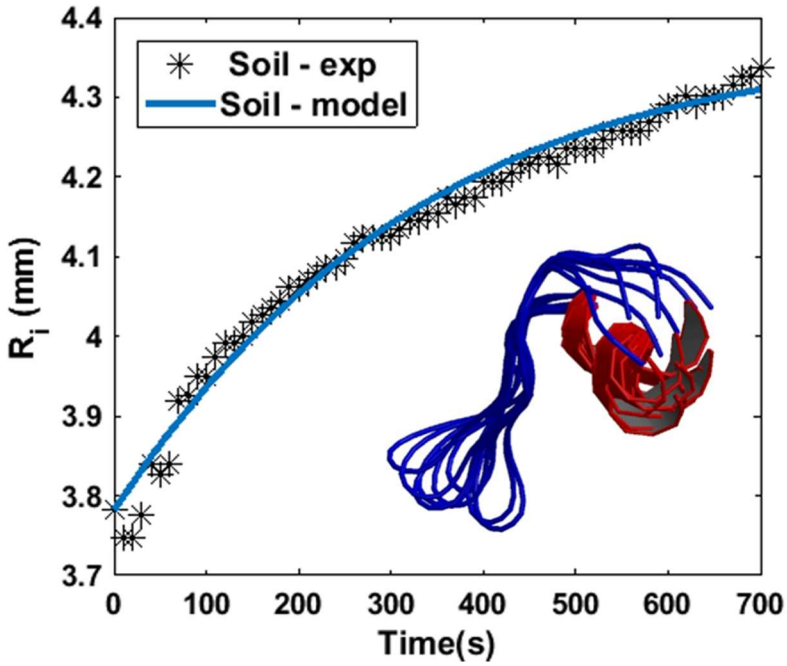

Figure 36 Digest model fit for soil at k_{cat} = 0.00152 s^{-1}(soil basis) and D = $1.2 \cdot 10^{-6}$ cm^2/s.

This activity measure is higher than that reported by standard, tyrosine release assays[57,88,89] due to the observation of film degradation rather than digestion to the extent of single monomers. An additional study would need to be performed to correlate this new method to existing hydrolytic assays. At this stage, we approximated in field testing by 3D printing a case capable of isolating the resonator from the soil environment. It includes a tray for the resonator (Fig 37I) and accompanying cap (Fig 37II) that when connected isolates the resonator from the surrounding soil and water dielectric and provides a small channel for the analyte. To improve casting of the substrate, we also include a spacer (Fig 37III) that can be inserted into the center well (Fig 37IV) and allows for the casting of the gel. This is then removed for testing (Fig 37V).

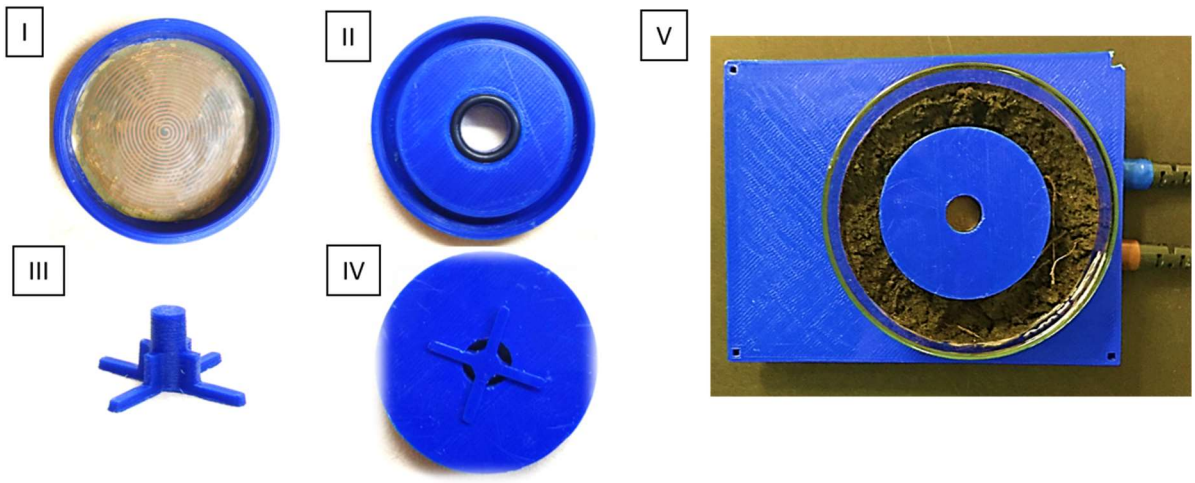

Figure 37 Plastic casing used to isolate resonator in soil tests.

CHAPTER 5. CONCLUSION AND FUTURE WORK

Inexpensive, flexible, wireless, resonant sensors can be rapidly fabricated using copper-coated polyimide substrate using indelible markers and an XY plotter. The frequency response window of the scattering parameter responses can be tuned by the resonator geometry and it is found that the 1-100MHz frequency range provides a clean spectral background and sufficient signal penetration through soil and water. A change in the relative permittivity on the resonator surface significantly shifts the reported, resonant frequency.

The activity of a hydrolytic enzyme can be measured by coating the surface of the resonator with a specific substrate to the enzyme and observing the degradation rate of the substrate as transduced wirelessly by a change in resonant frequency. This was demonstrated with Subtilisin A and bacterial protease mixtures that were dosed on resonators at varying enzyme concentrations. The experimental data can be fitted with a custom transport, reaction model to extract the catalytic activities (turnover rate or k_{cat}) for the enzyme. The sensors can be used to transduce enzyme activity in closed environments, as demonstrated by wireless measurement of soil proteolytic activity.

In future work, the resonant sensor packaging will be improved to allow for robust, *in situ* soil experiments for field studies of spatial and temporal dynamics of soil hydrolytic enzymes. Sensors for contact-free measurement for enzyme activity may also find utility in other applications such as bioreactors (*e.g.* activity of biocatalyst being produced) and wound management (*e.g.* lysozyme activity). Moreover, while the present work focused on

hydrolytic enzymes, future work could also encompass other types of enzymes such as ligases and lyases.

Although this study provides valuable information about the measurement of soil hydrolytic activity, we should consider the fact that the hydrolytic activity is not the only key indicator of soil health. It is also important to measure the concentration of specific ions, such as potassium and ammonium, which are essential for soil health and plant growth in the farm fields. Therefore, one potential direction for the future research can be wireless detection and measurement of different ion concentrations in a closed system for agricultural purposes using spiral resonators. The hypothesis for this research is that the resonators show ion specific responses which are affected by the resonator geometry. The conducted proof-of-concept tests regarding the ion concentration monitoring are presented here.

A panel of nine spiral Archimedean resonators with different geometries was designed in order to test the effect of resonator geometry on the ion specific sensor response (Table 5).

Table 5 Resonator geometry panel used for KCl and different ionic compounds(*).

	Pitch (mm)	Length (mm)	Outer Diameter (mm)
Constant Length	1	1255	40
	1.2	1255	43.81
	1.6	1255	50.59
	2	1255	56.54
	2.5	1255	63.21
Constant Pitch	1.2*	800	35
	1.2*	1255	43.81
	1.2	1324	45
	1.2	1979	55
	1.2*	2764	65

For the initial test, the resonator with 40mm diameter and 1mm pitch was selected and epoxied to the petri dish and then positioned at the center of the reader. Initially, 50ml DI water was added and then increasing concentrations of KCl was monitored while the overall volume was kept constant at 50ml in order to eliminate the effect of liquid volume on the sensor response. The magnitude of S_{21} was reordered vs frequency and a detectable change in resonant peak frequency, peak amplitude, and width was observed for different KCl concentration range (μM to M) which can be seen in Fig 38. The red circle, black x mark, and red dotted line represent the resonant peak, resonant trough, and the peak height, respectively.

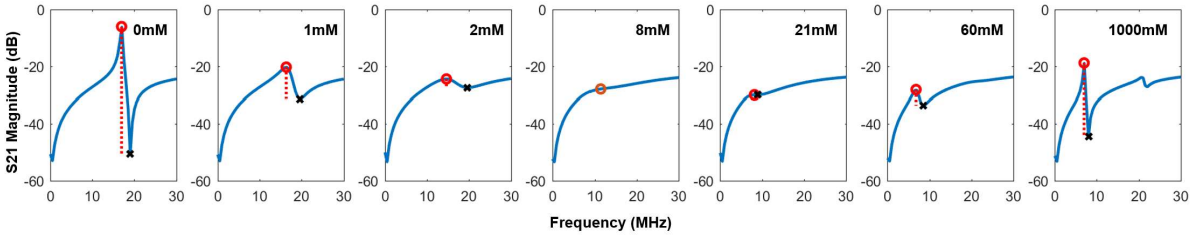

Figure 38 S_{21} magnitude (dB) response to KCl added to 40mm diameter, 1mm pitch resonators.

In order to test the effect of geometry on the sensor response, we repeated the KCl test for all 9 resonators presented in Table 5 and compared the changes in (a) resonant frequency peak, (b) amplitude, and (c) width for different sensor geometries (Fig 39 and Fig 40). The shift in all three parameters was similar; however, the magnitude and shape of these shifts were dependent on the resonator geometry.

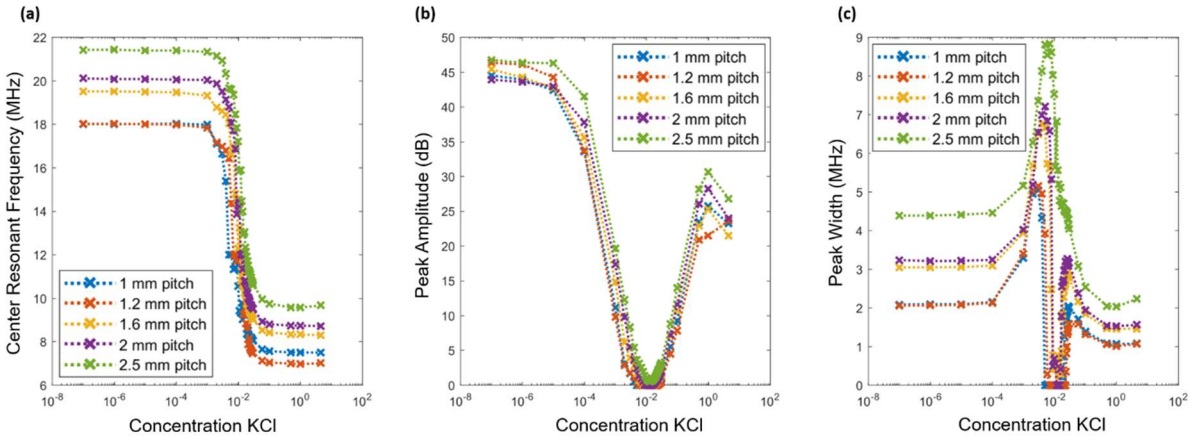

Figure 39 Effect of resonator geometry on the sensor S_{21} response to KCl concentrations for resonators with constant length and different pitch sizes.

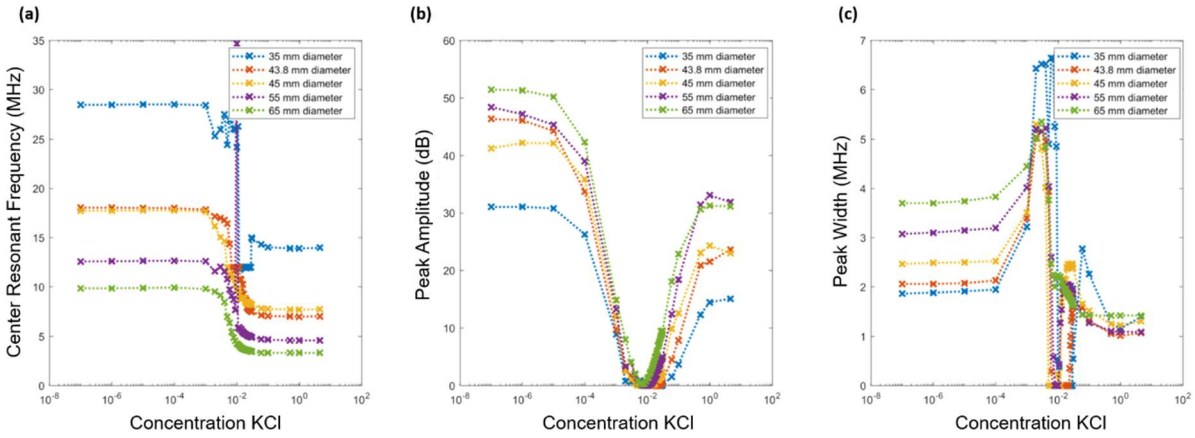

Figure 40 Effect of resonator geometry on the sensor S_{21} response to KCl concentrations for resonators with constant pitch and different length sizes.

For the final proof-of-concept test, we tested the ability of the sensor of having a particular response for different ions (having an ion-specific response). Ammonium Nitrate, Monoammonium Phosphate, Potassium Nitrate, and Monopotassium Phosphate (table 6) were the four salts tested on the resonators denoted with (*) in table 5.

Table 6 Salt panel for testing ion selectivity response of the resonant sensors.

Salt	Cation	Anion
Ammonium Nitrate	NH_4	NO_3
Monoammonium Phosphate	NH_4	PO_4
Potassium Nitrate	K	NO_3
Monopotassium Phosphate	K	PO_4

The phase and the magnitude of S_{21} for these three resonators with constant pitch sizes (1.2mm) and different lengths were plotted for the above-mentioned salts (Fig 41).

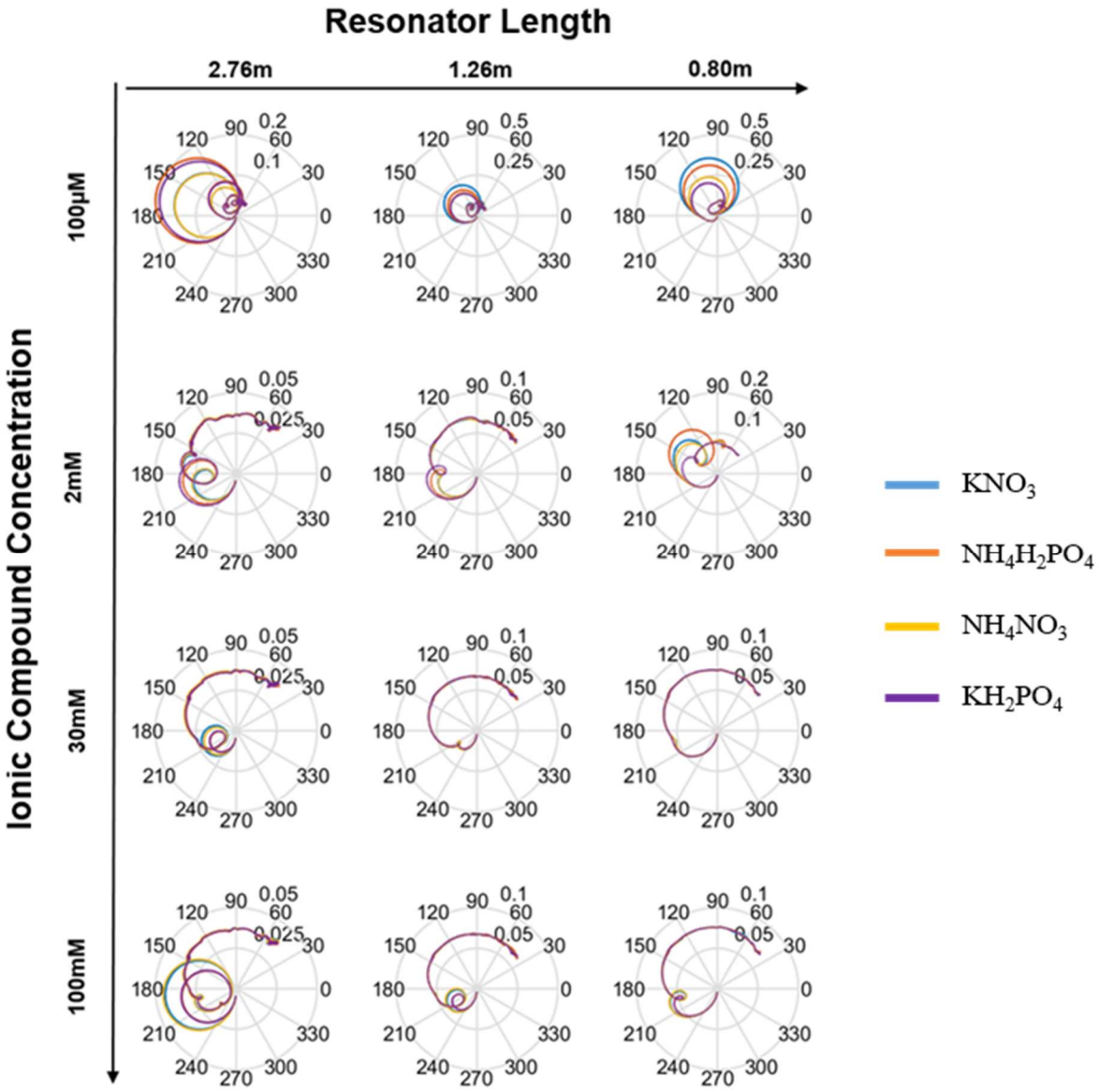

Figure 41 S_{21} magnitude and phase presented in polar plots for four different ionic compounds.

Having these preliminary results in hand, the main objective for the future research will be designing selective ion resonant sensors for recognition and quantification of the target ion in the presence of other competitive ions in closed systems.

REFERENCES

1. Clark, L. C. & Lyons, C. Electrode systems for continuous monitoring in cardiovascular surgery. *Ann. N. Y. Acad. Sci.* **102,** 29–45 (1962).

2. Grieshaber, D., MacKenzie, R., Vörös, J. & Reimhult, E. Electrochemical Biosensors - Sensor Principles and Architectures. *Sensors* **8,** 1400–1458 (2008).

3. Krco, S. Bluetooth Based Wireless Sensor Networks – Implementation Issues and Solutions. *Telekomun. Forum* 7 (2002).

4. Wang, N., Zhang, N. & Wang, M. Wireless sensors in agriculture and food industry - Recent development and future perspective. *Comput. Electron. Agric.* **50,** 1–14 (2006).

5. Saiya-Cork, K. ., Sinsabaugh, R. . & Zak, D. . The effects of long term nitrogen deposition on extracellular enzyme activity in an Acer saccharum forest soil. *Soil Biol. Biochem.* **34,** 1309–1315 (2002).

6. DeForest, J. L. The influence of time, storage temperature, and substrate age on potential soil enzyme activity in acidic forest soils using MUB-linked substrates and l-DOPA. *Soil Biol. Biochem.* **41,** 1180–1186 (2009).

7. Coulet, Pierre R.; Blum, L. J. Biosensor principles and applications. *Bioprocess technology* **15,** 1–344 (1991).

8. Ducheyne, P., Healy, K. E., Grainger, D. W., Hutmacher, D. W. & Kirkpatrick, C. J. Comprehensive biomaterials. *Comprehensive Biomaterials* **1,** 1–3363 (2011).

9. Gomes, M. T. S. R., Yurish, S. Y. & North Atlantic Treaty Organization. Scientific Affairs Division. Smart sensors and MEMS. *NATO science series. Series II, Mathematics, physics, and chemistry* xv, 480 (2004).

10. Kiekens, P. & Jayaraman, S. *Intelligent Textiles and Clothing for Ballistic and NBC Protection: Technology at the Cutting Edge*. (Springer Netherlands, 2012).

11. Thevenot, D. R. ELECTROCHEMICAL BIOSENSORS : RECOMMENDED Electrochemical biosensors : Recommended de ® nitions and classi ® cation (Technical Report). *Pure Appl. Chem.* **71,** 2333–2348 (1999).

12. Damborsky, P., vitel, J. & Katrlik, J. Optical biosensors. *Essays Biochem.* **60,** 91–100 (2016).

13. Mouffouk, F. *et al.* Development of a highly sensitive bacteria detection assay using fluorescent pH-responsive polymeric micelles. *Biosens. Bioelectron.* **26,** 3517–3523 (2011).

14. Janata, J. & Bezegh, A. Chemical Sensors. *Anal. Chem.* **60,** 62–74 (1988).

15. Wanekaya, A. K., Chen, W., Myung, N. V. & Mulchandani, A. Nanowire-based electrochemical biosensors. *Electroanalysis* **18,** 533–550 (2006).

16. Song, S., Wang, L., Li, J., Fan, C. & Zhao, J. Aptamer-based biosensors. *TrAC - Trends Anal. Chem.* **27,** 108–117 (2008).

17. Chen, Y., Liu, X., Wu, N. & Fierke, C. A. *Fluorescence-based real-time activity assays to identify RNase P inhibitors*. *Methods in Molecular Biology* **1520,** (2017).

18. Wang, L., Sipe, D. M., Xu, Y. & Lin, Q. A MEMS thermal biosensor for metabolic monitoring applications. *J. Microelectromechanical Syst.* **17,** 318–327 (2008).

19. Ramanathan, K. & Danielsson, B. Principles and applications of thermal biosensors. *Biosens. Bioelectron.* **16,** 417–423 (2001).

20. Acton, Q. A. *Advances in Bionanotechnology Research and Application: 2013 Edition*. (ScholarlyEditions, 2013).

21. Endo, H. *et al.* Wireless monitoring of blood glucose levels in flatfish with a needle biosensor. *Fish. Sci.* **76,** 687–694 (2010).

22. Narayan, R. J. *Medical Biosensors for Point of Care (POC) Applications*. (Elsevier Science, 2016).

23. Rida, A., Yang, L. & Tentzeris, M. *RFID-Enabled Sensor Design and Applications*. (Artech House, 2010).

24. Jones, E. C. & Chung, C. A. *RFID in Logistics: A Practical Introduction*. (CRC Press, 2007).

25. Oliveros, M. *et al.* Sensors and Actuators B : Chemical Photosensitive chipless radio-frequency tag for low-cost monitoring of light-sensitive goods. **223,** 839–845 (2016).

26. Curty, J. P., Declercq, M., Dehollain, C. & Joehl, N. *Design and Optimization of Passive UHF RFID Systems*. (Springer US, 2006).

27. Finkenzeller, K. & M?ller, D. *RFID Handbook: Fundamentals and Applications in Contactless Smart Cards, Radio Frequency Identification and Near-Field Communication*. (Wiley, 2010).

28. Yang, L., Zhang, R., Staiculescu, D., Wong, C. P. & Tentzeris, M. M. A novel conformal RFID-enabled module utilizing inkjet-printed antennas and carbon nanotubes for gas-detection applications. *IEEE Antennas Wirel. Propag. Lett.* **8,** 653–656 (2009).

29. Harpster, T. J., Stark, B. & Najafi, K. A passive wireless integrated humidity sensor. *Sensors Actuators, A Phys.* **95,** 100–107 (2002).

30. Sanz, D. A., Unigarro, E. A., Osma, J. F. & Segura-Quijano, F. Low cost wireless passive microsensors for the detection of hazardous compounds in water systems for control and monitoring. *Sensors Actuators, B Chem.* **178,** 26–33 (2013).

31. Strong, Z. A., Wang, A. W. & McConaghy, C. F. Hydrogel-actuated capacitive transducer for wireless biosensors. *Biomed. Microdevices* **4,** 97–103 (2002).

32. Preradovic, S. & Karmakar, N. Chipless RFID tag with integrated sensor. *Proc. IEEE Sensors* 1277–1281 (2010). doi:10.1109/ICSENS.2010.5690591

33. Ong, K. G., Grimes, C. A., Robbins, C. L. & Singh, R. S. Design and application of a wireless, passive, resonant-circuit environmental monitoring sensor. *Sensors Actuators, A Phys.* **93,** 33–43 (2001).

34. Reuel, N. F. *et al.* Hydrolytic Enzymes as (Bio)-Logic for Wireless and Chipless Biosensors. *ACS Sensors* **1,** 348–353 (2016).

35. Mavaddat, R. *Network Scattering Parameters*. (World Scientific, 1996).

36. Karris, S. T. *Circuit Analysis II: With MATLAB Applications*. (Orchard Publications, 2003).

37. Elbert, B. R. *The Satellite Communication Applications Handbook*. (Artech House, 2004).

38. Srinivasulu, P. & Vaidyanathan, C. V. *Handbook of Machine Foundations*. (Tata McGraw-Hill, 1976).

39. service)., I. X. (Online *et al. IEEE International Conference on Systems Engineering*. (Institute of Electrical and Electronics Engineers).

40. Zhuravel, A. P. *et al.* Imaging the paramagnetic nonlinear Meissner effect in nodal gap superconductor. **54504,** 1–14 (2017).

41. Mischke, C. R. Chapter 37. 755–772 (1999). doi:10.1007/978-1-61779-558-9

42. Purich, D. L. *Enzyme Kinetics: Catalysis and Control: A Reference of Theory and Best-Practice Methods*. (Elsevier Science, 2010).

43. Champe, P. C., Harvey, R. A. & Ferrier, D. R. *Biochemistry*. (Lippincott Williams & Wilkins, 2005).

44. Li, S., Yang, X., Yang, S., Zhu, M. & Wang, X. Technology Prospecting on Enzymes: Application, Marketing and Engineering. *Comput. Struct. Biotechnol. J.* **2,** e201209017 (2012).

45. Singh, R., Kumar, M., Mittal, A. & Mehta, P. K. Microbial enzymes: industrial progress in 21st century. *3 Biotech* **6,** 1–15 (2016).

46. Girisham, S., Reddy, S. R. & Charya, M. A. S. *Microbial Diversity : Exploration & Bioprospecting:* (SCIENTIFIC PUBLISHER (IND., 2012).

47. Sanchez, S. & Demain, A. L. Enzymes and bioconversions of industrial, pharmaceutical, and biotechnological significance. *Org. Process Res. Dev.* **15,** 224–230 (2011).

48. Ribeiro, D. S., Henrique, S. M. B., Oliveira, L. S., Macedo, G. A. & Fleuri, L. F. Enzymes in juice processing: A review. *Int. J. Food Sci. Technol.* **45,** 635–641 (2010).

49. Fernandes, P. Enzymes in Food Processing: A Condensed Overview on Strategies for Better Biocatalysts. *Enzyme Res.* **2010,** 1–19 (2010).

50. Kirk, O., Borchert, T. V. & Fuglsang, C. C. Industrial enzyme applications. *Curr. Opin. Biotechnol.* **13,** 345–351 (2002).

51. Boominadhan, U. *et al.* Optimization of Protease Enzyme Production Using Bacillus Sp . Isolated from Different Wastes. *Bot. Res. Int.* **2,** 83–87 (2009).

52. Burns, R. G. Enzyme activity in soil: Location and a possible role in microbial ecology. *Soil Biol. Biochem.* **14,** 423–427 (1982).

53. Tabatabai, M. A. Soil Enzymes. in *Encyclopedia of Environmental Microbiology* (John Wiley & Sons, Inc., 2003). doi:10.1002/0471263397.env211

54. McDaniel, M. D. & Grandy, A. S. Soil microbial biomass and function are altered by 12 years of crop rotation. *SOIL Discuss.* 1–39 (2016). doi:10.5194/soil-2016-39

55. Soil Enzyme Activities as Biological Indicators of Soil Health . *Reviews on Environmental Health* **18,** 65 (2003).

56. Allison, S. D. & Vitousek, P. M. Responses of extracellular enzymes to simple and complex nutrient inputs. *Soil Biol. Biochem.* **37,** 937–944 (2005).

57. Geisseler, D. & Horwath, W. R. Regulation of extracellular protease activity in soil in response to different sources and concentrations of nitrogen and carbon. *Soil Biol. Biochem.* **40,** 3040–3048 (2008).

58. Frankenberger, W. & Dick, W. Relationships Between Enzyme Activities and Microbial Growth and Activity Indices in Soil1. *Soil Sci. Soc. Am. J. - SSSAJ* **47,** (1983).

59. German, D. P. *et al.* Optimization of hydrolytic and oxidative enzyme methods for ecosystem studies. *Soil Biol. Biochem.* **43,** 1387–1397 (2011).

60. Schloter, M., Nannipieri, P., Sørensen, S. J. & Elsas, J. D. Van. Microbial indicators for soil quality. 1–10 (2018).

61. Tan, X. *et al.* County-Scale Spatial Distribution of Soil Enzyme Activities and Enzyme Activity Indices in Agricultural Land: Implications for Soil Quality Assessment. *Sci. World J.* **2014,** 1–11 (2014).

62. Acosta-Martínez, Verónica & Tabatabai, M. Ali. Methods of Soil Enzymology. *Methods Soil Enzymol.* **sssabookse,** 161–183 (2011).

63. Bell, C. W. *et al.* High-throughput Fluorometric Measurement of Potential Soil Extracellular Enzyme Activities. *J. Vis. Exp.* 1–16 (2013). doi:10.3791/50961

64. Buroker-Kilgore, M. & Wang, K. K. W. A coomassie brilliant blue G-250-based colorimetric assay for measuring activity of calpain and other proteases. *Analytical Biochemistry* **208,** 387–392 (1993).

65. Kushner, N. N., Riggin, C. H., Annunziato, M. E. & Marciani, D. J. Fluorometric enzyme immunoassay for measurement of infectious feline leukemia virus and its neutralization. *J. Immunol. Methods* **114,** 253–260 (1988).

66. Ahamed, A. & Vermette, P. Culture-based strategies to enhance cellulase enzyme production from Trichoderma reesei RUT-C30 in bioreactor culture conditions. *Biochem. Eng. J.* **40,** 399–407 (2008).

67. Lozano, P. *et al.* Bioreactors based on monolith-supported ionic liquid phase for enzyme catalysis in supercritical carbon dioxide. *Adv. Synth. Catal.* **349,** 1077–1084 (2007).

68. Qi, Q. *et al.* Properties of humidity sensing ZnO nanorods-base sensor fabricated by screen-printing. *Sensors Actuators, B Chem.* **133,** 638–643 (2008).

69. Ping, J., Wu, J., Wang, Y. & Ying, Y. Simultaneous determination of ascorbic acid, dopamine and uric acid using high-performance screen-printed graphene electrode. *Biosens. Bioelectron.* **34,** 70–76 (2012).

70. Secor, E. B., Prabhumirashi, P. L., Puntambekar, K., Geier, M. L. & Hersam, M. C. Inkjet printing of high conductivity, flexible graphene patterns. *J. Phys. Chem. Lett.* **4,** 1347–1351 (2013).

71. Je, S. S., Sharma, T., Lee, Y., Gill, B. & Zhang, J. X. A thin-film piezoelectric PVDF-TrFE based implantable pressure sensor using lithographic patterning. *Proc. IEEE Int. Conf. Micro Electro Mech. Syst.* 644–647 (2011). doi:10.1109/MEMSYS.2011.5734507

72. Potyrailo, R. A. & Surman, C. A Passive Radio-Frequency Identification (RFID) Gas Sensor With Self-Correction Against Fluctuations of Ambient Temperature. *Sens. Actuators. B. Chem.* **185,** 587–593 (2013).

73. Occhiuzzi, C., Cippitelli, S. & Marrocco, G. Modeling, design and experimentation of wearable RFID sensor tag. *IEEE Trans. Antennas Propag.* **58,** 2490–2498 (2010).

74. Halliday, D., Resnick, R. & Walker, J. *Fundamentals of Physics, Chapters 33-37*. (Wiley, 2010).

75. Benelli, G. & Pozzebon, A. RFID Under Water: Technical Issues and Applications. in *Radio Frequency Identification from System to Applications* (ed. Reaz, M. B. I.) (InTech, 2013). doi:10.5772/53934

76. Jiang, S. & Georgakopoulos, S. Electromagnetic Wave Propagation into Fresh Water. *J. Electromagn. Anal. Appl.* **3,** 261–266 (2011).

77. Deen, W. M. *Analysis of Transport Phenomena*. (OUP USA, 2012).

78. Sadov, S. Y., Shivakumar, P. N., Firsov, D., Lui, S. H. & Thulasiram, R. Mathematical Model of Ice Melting on Transmission Lines. *J. Math. Model. Algorithms* **6,** 273–286 (2007).

79. Blasik, M. Numerical scheme for the one-phase 1D Stefan problem using curvilinear coordinates. *Sci. Res. Inst. Math. Comput. Sci.* **11,** 9–14 (2012).

80. Boureghda, A. Solution to an ice melting cylindrical problem. *J. Nonlinear Sci. Appl* **9,** 1440–1452 (2016).

81. Steven C. Chapra, D. *Applied Numerical Methods with MATLAB for Engineers and Scientists*. (McGraw-Hill Education, 2017).

82. Brune, D. & Kim, S. Predicting protein diffusion coefficients. *Proc. Natl. Acad. Sci.* **90,** 3835–3839 (1993).

83. Sil, P. C., Chaudhuri, T. K. & Sinha, N. K. Basic trypsin-subtilisin inhibitor from marine turtle egg white: Hydrodynamic and inhibitory properties. *J. Protein Chem.* **12,** 71–78 (1993).

84. Schwert, G. W. The Molecular Size and Shape of the Pancreatic Proteases. *J. Biol. Chem.* **179,** 655–664 (1949).

85. Sutter, M., Siepmann, J., Hennink, W. E. & Jiskoot, W. Recombinant gelatin hydrogels for the sustained release of proteins. *J. Control. Release* **119,** 301–312 (2007).

86. Kobza, J. & Seemann, J. R. Light-dependent kinetics of 2-carboxyarabinitol 1-phosphate metabolism and ribulose-1,5-bisphosphate carboxylase activity in vivo. *Plant Physiol.* **89,** 174–179 (1989).

87. Society, B. E. Effects of Timing of Nutrient Addition on Competition Within and Between Two Annual Plant Species Author (s): B . L . Benner and F . A . Bazzaz Published by : British Ecological Society Stable URL : http://www.jstor.org/stable/2260548 REFERENCES Linked . **75,** 229–245 (2018).

88. Baran, S., Bielińska, J. E. & Oleszczuk, P. Enzymatic activity in an airfield soil polluted with polycyclic aromatic hydrocarbons. *Geoderma* **118,** 221–232 (2004).

89. Pascual, J. A., Garcia, C., Hernandez, T., Moreno, J. L. & Ros, M. Soil microbial activity as a biomarker of degradation and remediation processes. *Soil Biol. Biochem.* **32,** 1877–1883 (2000).

APPENDIX. MATLAB SCRIPTS

The following Matlab codes are attributed to Prof. Nigel Reuel.

1. Matlab Code for VNA Signal Capture

An S5048 two-port vector network analyzer from Copper Mountain Technologies was used to measure the resonant sensor scattering parameters. The code below interfaces with the VNA for taking S_{21} data at 15s intervals for three hours via Matlab.

```
function VNADataGrab
% Coded by Nigel F. Reuel on 7.22.2105
% This code interfaces with the copper mountain VNA and takes data at
%specified intervals

Exptime = 10800; %sec
Interval = 15; %sec
Npts = round(Exptime/Interval);
for i = 1:Npts
    tic
    [F,Yavg] = vna('S5048',[],55e6,85e6,4000,[],'S21');
    % Insert save function here....what does the data look like from
    if i == 1
        csvwrite('FreqVector.csv',F) % Write the frequency vector on the
first run...
    end
    csvwrite(['Ydata_',int2str(i),'.csv'],Yavg)
     m = 10;
    t = toc;
    pause(Interval-t);

end
end

%%%%%%%%%%%%%%%%%%%%%%%%%%%%%%%%%%%%%%%%%%%%%%%%%%%%%%%%%%%%%%%%%%%%%%%%%%%%
%%%
%  MATLAB programming example for Copper Mountain VNA
%
%  Version:  1.0
%
%  Author:  Ben Maxson, Copper Mountain Technologies
%           ben.m@coppermountaintech.com
%
%  Support:  support@coppermountaintech.com
%
%%%%%%%%%%%%%%%%%%%%%%%%%%%%%%%%%%%%%%%%%%%%%%%%%%%%%%%%%%%%%%%%%%%%%%%%%%%%
%%%
%   Function syntax is as shown below.  [Default] arguments are used if
%   omitted.
%   Usage examples:
```

```
%   >> vna('S5048')
%
%   >> vna('Planar804',0,10e6,6e9,801)
%
%   >> vna('R54',[],[],[],1601,[],'S11')
%
% function output = vna(...
%   instrument,...          %'S5048','S7530','Planar804','Planar304',
%     ...                     %  'S8081' (Planar808/1), 'R54', 'R140',
%     ...                     %  ['TR1300'], 'TR5048', or 'TR7530'
%   use_center_and_span,... %[false] = use fstart/fstop, true = use
center/span
%     f1_hz,...               %[fstart=400e6] or center, as per above, in
Hz
%     f2_hz,...               %[fstop=600e6] or span, as per above, in Hz
%     num_points,...          %[401] number of measurement points
%     power_level_dbm,...     %[0] dBm power level (ignored for R54/140)
%     parameter,...           %['S11'], 'S12', 'S22', etc. R54/140 must
use
%     ...                     %  'S11'; TR devices must use 'S11' or
'S21';
%     ...                     %  Ports 3 and 4 available for S8081 only
%     format,...              %['mlog'] or 'phase'
%     time_per_iter_sec,...   %[1.0] seconds per measurement interval
%     num_iter,...            %[10] number of times to loop
%     num_iter_to_store...    %[1] number of function iterations to store)

function [F,Yavg] = vna(...
    instrument,...          %'S5048','S7530','Planar804','Planar304',
    ...                     %  'S8081' (Planar808/1), 'R54', 'R140',
    ...                     %  ['TR1300'], 'TR5048', or 'TR7530'
    use_center_and_span,... %[false] = use fstart/fstop, true = use
center/span
    f1_hz,...               %[fstart=400e6] or center, as per above, in Hz
    f2_hz,...               %[fstop=600e6] or span, as per above, in Hz
    num_points,...          %[401] number of measurement points
    power_level_dbm,...     %[0] dBm power level (ignored for R54/140)
    parameter,...           %['S21'], 'S11', 'S12', etc. R54/140 must use
    ...                     %  'S11'; TR devices must use 'S11' or 'S21';
    ...                     %  Ports 3 and 4 available for S8081 only
    format,...              %['mlog'] or 'phase'
    time_per_iter_sec,...   %[1.0] seconds per measurement interval
    num_iter,...            %[10] number of times to loop
    num_iter_to_store...    %[2] number of function iterations to store
    )
    %%%%%%%%%%%%%%%%%%%%%%%%%%%%%%%%%%%%%%%%%%%%
    %
    %  Assign default parameters to missing
    %   or empty input arguments
    %
    % instrument = 'TR1300'
    if ~exist('instrument','var')
        instrument = 'TR1300';
    elseif isempty(instrument)
        instrument = 'TR1300';
    end
    % use_fcenter_and_fspan = 'false'
```

```
if(~exist('use_fcenter_and_fspan','var'))
    use_fcenter_and_fspan = false;
elseif isempty(use_fcenter_and_fspan)
    use_fcenter_and_fspan = false;
end

% f1_hz = 400e6
if(~exist('f1_hz','var'))
    f1_hz = 400e6;
elseif isempty(f1_hz)
    f1_hz = 400e6;
end

% f2_hz = 600e6
if(~exist('f2_hz','var'))
    f2_hz = 600e6;
elseif isempty(f2_hz)
    f2_hz = 600e6;
end

% num_points = 401
if(~exist('num_points','var'))
    num_points = 4000;
elseif isempty(num_points)
    num_points = 4000;
end

% power_level_dbm = 0
if(instrument(1) ~= 'R')
    if(~exist('power_level_dbm','var'))
        power_level_dbm = 0;
    elseif isempty(power_level_dbm)
        power_level_dbm = 0;
    end
end

% parameter = 'S11'
if(~exist('parameter','var'))
    if(instrument(1) ~= 'R')
        parameter = 'S21';
    else
        parameter = 'S11';
    end
elseif isempty(parameter)
    if(instrument(1) ~= 'R')
        parameter = 'S21';
    else
        parameter = 'S11';
    end
end

% format = 'mlog'
if(~exist('format','var'))
    format = 'mlog';
elseif isempty(format)
    format = 'mlog';
```

```
end

% time_per_iter_sec = 1.0
if(~exist('time_per_iter_sec','var'))
    time_per_iter_sec = 1.0;
elseif isempty(time_per_iter_sec)
    time_per_iter_sec = 1.0;
end

% num_iter = 10
if(~exist('num_iter','var'))
    num_iter = 10;
elseif isempty(num_iter)
    num_iter = 10;
end

% num_iter_to_store = 2
if(~exist('num_iter_to_store','var'))
    num_iter_to_store = 1;
elseif isempty(num_iter_to_store)
    num_iter_to_store = 1;
end
%%%%%%%%%%%%%%%%%%%%%%%%%%%%%%%%%%%%%%%%%%%%
%
%  Example code
%
%Instantiate COM client
try
    app=actxserver([instrument,'.application']);
catch ME
    disp('Error establishing COM server connection.');
    disp('Check that the VNA application COM server was registered')
    disp('at the time of software installation.');
    disp('This is described in the VNA programming manual.');
    return
end

%Wait up to 20 seconds for instrument to be ready
ready = 0;
count = 0;
while ~ready
    ready = app.ready;
    if count>20,
        disp('Error, instrument not ready.');
        disp('Check that VNA is powered on and connected to PC.');
        disp('The status Ready should appear in the lower right');
        disp('corner of the VNA application window.');

        return
    end;

    %Check every so often whether the instrument is ready yet
    pause(1)
    count = count + 1;
end
```

```
    %Get and echo the instrument name, serial number, etc.
    %
    %  [This is a simple example of getting a property in MATLAB.]
    %
    disp(sprintf(app.name));

    %Set the instrument to a Preset state
    %
    %  [This is an example of executing an ActiveX "method" in MATLAB.]
    %
    invoke(app.scpi.system,'preset');

    %Configure the stimulus
    if use_fcenter_and_fspan
        %
        % [This is an example of getting and setting a property with
nested get
        % statements. Nested gets are needed when an indexed parameter is
        % used (app.scpi.sense[1] in this case).]
        %
set(get(get(get(get(app.scpi,'sense',1),'frequency'),'center'),f1_hz));

set(get(get(get(get(app.scpi,'sense',1),'frequency'),'span'),f2_hz));
    else
        %
        % [This is an example of getting and setting a property with the
        % subfunction multiget().
        %
        set(multiget(app,'scpi','sense',1,'frequency'),'start',f1_hz);
        set(multiget(app,'scpi','sense',1,'frequency'),'stop',f2_hz);
    end

    set(multiget(app,'scpi','sense',1,'sweep'),'points',num_points);

    if(instrument(1) ~= 'R')

set(multiget(app,'scpi','source',1,'power','port',1,'level','immediate'),'
amplitude',power_level_dbm);
    end

    %Configure the measurement

set(multiget(app,'scpi','calculate',1,'parameter',1),'define',parameter);
    set(multiget(app,'scpi','calculate',1,'selected'),'format',format);
    set(multiget(app,'scpi','trigger','sequence'),'source','bus');

    tic;
    Yavg = zeros(1,num_points);
    for iter = 1:num_iter

        %Execute the measurement
        invoke(app.scpi.trigger.sequence,'single');

        Y =
```

```
get(get(get(get(app.scpi,'calculate',1),'selected'),'data'),'fdata');
        Y = Y(1:2:end);
        Yavg = Yavg + Y;
        F = get(get(get(app.scpi,'sense',1),'frequency'),'data');

        while(toc<iter*time_per_iter_sec)
            pause(0.01);
        end

    end
Yavg = Yavg./num_iter;
end

function out = multiget(varargin)


    if(nargin==0)           % Nothing to get
        return
    elseif(nargin==1)       % Return the object itself
        out = varargin{1};
    else
        out = varargin{1};  % At least one property is passed in
        idx = 2;
        while idx <= nargin

            %There are at least 2 more arguments not year processed
            if( (nargin - idx) >= 1)

                %If the latter is a number, get the indexed property
                if( isnumeric(varargin{idx+1}))
                    out = get(out,varargin{idx},varargin{idx+1});
                    idx = idx+2;
                    continue;
                end
            end

            %Last argument, or next one's not a number, so there's no
index
            %Just get the property itself
            out = get(out,varargin{idx});
            idx = idx+1;

        end

 end
```

2. Matlab Code for Resonant Frequency Detection

The code below was used for detecting the resonant frequency of the sensor which was defined as the peak of the S_{21} magnitude sigmoidal response of the resonator.

```
function CirclePeakWithVNAgrab_V2
% Note: All the RF values are saved in PeakFreq.csv

nfile = 2880;
for i = 1:nfile

    Y = csvread(['Ydata_',int2str(i),'.csv']); %savetrace data
    X = csvread('FreqVector.csv')./10^6;
    [Y2,pos] = findpeaks(Y); %Find all the potential peak and record
vector location
     if isempty(Y2)  %Click peak is activated in case no peaks can be
found by matlab
        plot(X,Y)
        hold on
    ylim([-60 0])
    xlim([1 100])
    ylabel('S21 (dB)')
    xlabel('Frequency (MHz)')
    [RF,S21_Val] = ginput(1);
    plot(RF,S21_Val,'o')
    hold off
    hgexport(gcf, ['Plot_',int2str(i),'.jpg'], hgexport('factorystyle'),
'Format', 'jpeg');
        PeakFreq(i)= RF;
        csvwrite('PeakFreq.csv',PeakFreq)
     else
       X2 = X(1,pos);   %Selected FreqVec corresponding to each potential
peak
        [Peak,pos2] = max(Y2); %Find max peak and record the vector
location
    Freqloc = X2(1,pos2);

    plot(X,Y);
    ylim([-60 0])
    xlim([55 85])
    ylabel('S21 (dB)')
    xlabel('Frequency (MHz)')
    hold on
    plot(Freqloc,Peak,'o')
    hold off
    hgexport(gcf, ['Plot_',int2str(i),'.jpg'], hgexport('factorystyle'),
'Format', 'jpeg');
    PeakFreq(i) = Freqloc;
    csvwrite('PeakFreq.csv',PeakFreq)
     end
end
```

3. Code for the Numerical Model

The numerical model was solved using Matlab with the following code:

```
function O = GelSimulator(kcat,CE)
% Coded by NFR on 11.20.2017
% Digestion model as described in paper
% Inputs:
```

```
%   kcat = turnover frequency (s^-1) for enzyme
%   CE = starting concentration of enzyme in center well (g/ml)
% Outputs:
%   O = two column vector, first column = time (s), second column = radius
%   (mm) of digestion front on gel corresponding to the time
% Model constants
Din = 3.7821*2/10; %cm - Diameter of well in center of substrate
Dout = 6.25*2/10; %cm - Diameter of substrate puck
h = 0.001; %cm - step size of mesh [default 0.01mm]
rvec = (Din/2:h:Dout/2)';
Dif_g = 1.2*10^-6; %cm^2/s estimate from 1980 paper
% Initialize concentration along mesh
Co = zeros(length(rvec),1);
to = 0;
delt = 1; % Time step resolution (0.5 to 1, smaller = longer solution
time)
tp_record = [];
yp_record = [];
tend = 800; % Built in end time of simulation
i = 1;
VolDigest_Vec = pi*(rvec.^2-(rvec-h).^2).*0.067;
%NOTE: Volume of the model 'rings' specified by node spacing;
% last number is height of gel(cm)calculated assuming level(30ul)add at
start
% Volume is of outer most ring, in cm^3
MD_o = (VolDigest_Vec*(0.14))'; % in grams, assuming 14wt% gelatin!
% Record timepoints at which different radii are
digested,C1=time,C2=radius (mm)
Report = [0 rvec(1)*10]; % Record the radius in mm
cf = 1;
while to < tend
    ti = to;
    dnf = 0; %digest node flag!
    % This while loop operates while there is still gel present in this
    % node to digest
    while dnf == 0
        ti = ti + delt;
        tspan = [to ti];
        [tp,yp] =
ode45(@GelPDE,tspan,Co(i:end,1),[],h,Dif_g,CE,rvec(i:end,1),VolDigest_Vec)
;
        % Calculate how much digested along the length of gel
        dt = diff(tp);
        dt = [dt; dt(end)];
        mdigest = sum(((yp.*dt)'.*VolDigest_Vec(i:end,1))').*kcat;
        if MD_o(1,i) - mdigest(1,1) <= 0
            dnf = 1;
            % This section has been digested! Record the time point
            Report = [Report; tp(end) rvec(cf)*10];
            cf = cf+1;
            % Also change the exterior CE, do this at line 68
        end
        %MD_o(1,i) - mdigest(1,1)
    end
    to = ti% %<-keep comment off to show progress of simulatorV8 no print
to make faster
    MD_o(1,i:end) = MD_o(1,i:end) - mdigest;
```

```
    if i > 1
        ExtraMat = CE.*ones(length(tp),i-1); % 1.24.17 NFR look at this...
    % radial portion of gel, value = concentration of enzyme at that point
        yp = [ExtraMat yp];
    end
    % tp = time points from ODE solver
    % yp = rows correspond to time points, columns = spatial points along
    yp_record = [yp_record; yp];
    tp_record = [tp_record; tp];
    Co = yp(end,:)';
    i = i+1;
    % Reflect the dilution effect of enzyme in center well:
    Eingel = sum(Co(i:end,1).*VolDigest_Vec(i:end,1));
    VolCenter = 30/1000+sum(VolDigest_Vec(1:i-1,1)); % 30ul added? Check
with Sadaf.  This is the VOLUME of liquid in center
    CE = (CE*VolCenter-Eingel)/VolCenter;
    %Co(1:i,1) = CE;
end
% Export the time points of the response (NOTE neglect first point as
% discussed in supplement)
TimeVec = Report(2:end,1)-Report(2,1);
Rvec = Report(2:end,2);
O = [TimeVec Rvec];
% End of model simulation.
end
 function dydt = GelPDE(t,C,h,Dif_g,CEo,rvec,Vvec)
% The enzyme concentration in center is NOT contstant for this small
volume
if t == 0
    CE = CEo;
else
   % For other times, we need to see how much has penetrated gel...
   nr = length(rvec);
   nV = length(Vvec);
   nd = nV-nr;
   Eingel = sum(C.*Vvec(nd+1:end,1));
   VolCenter = 30/1000+sum(Vvec(1:nd,1)); %This is VOLUME of liquid in
center
   CE = (CEo*VolCenter-Eingel)/VolCenter;
end
% Finite difference equations for all NODES
dydt = zeros(length(C),1);
dydt(1,1) = ((C(2,1)-2*C(1,1)+CE)/h^2+(1/rvec(1,1))*(C(2,1)-
CE)/(2*h))*Dif_g; % First spatial point with constant
for i = 2:length(C)-1
   dydt(i,1) = ((C(i+1)-2*C(i)+C(i-1))/h^2+(1/rvec(i,1))*(C(i+1,1)-C(i-
   1,1))/(2*h))*Dif_g; % Internal points
end
dydt(end,1) = (2*C(end-1,1)-2*C(end,1))/h^2*Dif_g;
No flux at end
End
```

4. Code for Bead Experiment Image Analysis

```
function VideoAnalysis
```

```
% Coded by NFR on 10.21.2017
% This code can analyze the web cam pictures of the gel to get the spatial
% response % Display the first picture
I = imread('Pic_1.png');
%figure('units','normalized','outerposition',[0 0 1 1])
imshow(I)
title('Click the UL and LR O-ring region to zoom.')
C = round(ginput(2));
close
% Now display the zoomed region and have user select 4 interior ring
% points:
%Ig = double(rgb2gray(I));
Igzoom = I(C(1,2):C(2,2),C(1,1):C(2,1),:);
imagesc(Igzoom)
R = round(ginput(4));
% Determine cetner point of o-ring
Cr1 = (R(2,2)-R(1,2))/2+R(1,2);
Cr2 = (R(4,2)-R(3,2))/2+R(3,2);
Cc1 = (R(2,1)-R(1,1))/2+R(1,1);
Cc2 = (R(4,1)-R(3,1))/2+R(3,1);
Cr = round((Cr1+Cr2)/2);
Cc = round((Cc1+Cc2)/2);
%hold on
%plot(Cc,Cr,'o') %Yes, verified this is the center point
close % Close zoomed image
% Calculate Diameter
D1 = sqrt((R(2,2)-R(1,2))^2+(R(4,2)-R(3,2))^2);
D2 = sqrt((R(2,1)-R(1,1))^2+(R(4,1)-R(3,1))^2);
D = (D1+D2)/2;
csvwrite('Diameter2.csv',D);
ni = 800; % Insert number of images to analyze here
% Preallocate vector for reaction front radius
rvec = zeros(ni,1);
for i = 14:ni
    I = imread(['Pic_',int2str(i),'.png']);
    %Ig = double(rgb2gray(I));
    Igzoom = I(C(1,2):C(2,2),C(1,1):C(2,1),:);
    imshow(Igzoom)
    imwrite(Igzoom,['Zoom_',int2str(i),'.png'])
    close
    imagesc(Igzoom)
    title('CLICK gel edge in 3 spots.')
    E = ginput(3);
    % Determine the radius of reaction front:
    r1 = sqrt((Cr-E(1,2))^2+(Cc-E(1,1))^2);
    r2 = sqrt((Cr-E(2,2))^2+(Cc-E(2,1))^2);
    r3 = sqrt((Cr-E(3,2))^2+(Cc-E(3,1))^2);
    rvec(i,1) = (r1+r2+r3)/3;
    csvwrite('rvec2.csv',rvec)
end

    end
```